Digital Signal Processing 48 (2016) 163–177

Contents lists available at ScienceDirect

Digital Signal Processing

www.elsevier.com/locate/dsp

Performance analysis of a family of adaptive blind equalization algorithms for square-QAM

Ali W. Azim [a,b], Shafayat Abrar [c,*], Azzedine Zerguine [d], Asoke K. Nandi [e]

[a] Institute Polytechnique de Grenoble Saint Martin d'Hères, 38400, France
[b] COMSATS Institute of Information Technology, Wah Cantt 47040, Pakistan
[c] COMSATS Institute of Information Technology, Islamabad 44000, Pakistan
[d] King Fahd University of Petroleum & Minerals, Dhahran 31261, Saudi Arabia
[e] Brunel University London, Uxbridge, Middlesex UB8 3PH, United Kingdom

ARTICLE INFO

Article history:
Available online 25 September 2015

Keywords:
Multimodulus algorithm
Blind equalization
Adaptive equalizers
Steady-state analysis
Receiver design
Convergence analysis

ABSTRACT

Multimodulus algorithms (MMA) based adaptive blind equalizers mitigate inter-symbol interference and recover carrier-phase in communication systems by minimizing dispersion in the in-phase and quadrature components of the received signal using the respective components of the equalized sequence in a decoupled manner. These equalizers are mostly incorporated in bandwidth-efficient digital receivers which rely on quadrature amplitude modulation (QAM) signaling. The nonlinearities in the update equations of these equalizers tend to lead to difficulties in the study of their steady-state performance. This paper presents originally the steady-state excess mean-square-error (EMSE) analysis of different members of multimodulus equalizers MMAp–q in a non-stationary environment using energy conservation arguments, and thus bypassing the need for working directly with the weight error covariance matrix. In doing so, the exact and approximate expressions for the steady-state mean-square-error of several MMA based blind equalization algorithms are derived, including MMA2–2, MMA2–1, MMA1–2, and MMA1–1. The accuracy of the derived analytical results is validated using Monte–Carlo experiments and found to be in close agreement.

1. Introduction

Blind equalizers mitigate different types of interferences such as inter-symbol interference (ISI), frequency selective fading, etc., caused by non-ideal transformations performed by the dispersive channels in a communication system. A blind adaptive equalizer attempts to compensate for the distortions of the channel by processing the received signals and reconstructing the transmitted signal up to some indeterminacies by the use of linear or nonlinear filters without any knowledge of the channel impulse response and without direct access to the transmitted sequence itself. The basic idea behind an adaptive blind equalizer is to minimize or maximize some admissible blind objective or cost function through the choice of filter coefficients based on the equalizer output [1–3].

The performance of an adaptive filter can be evaluated using transient and steady-state analyses. The former provides information about the stability and the convergence rate of an adaptive filter, whereas the latter provides information about the mean-square-error of the filter once it reaches steady state. In the steady-state analysis of adaptive filters, one of the properties to be considered is their ability to track changes/variations in the signal statistics of the received signal. This property is of significant importance, particularly in mobile communications systems and applications like acoustic echo cancellation, etc.

Blind adaptive filters (or equalizers) are based on recursive algorithms that allow the filter to adapt and track (slow) variations in input statistics. Such adaptive filters start from certain initial conditions without any prior knowledge about the input signal statistics, then the filter coefficients are updated based on the chosen adaptive algorithms and the sequence of the sampled data values. In stationary environments, adaptive filters converge to optimum Wiener solution [4–13]. However, in non-stationary environments, the optimum Wiener solution takes time-varying form that results in variation of saddle point in error performance sur-

* Corresponding author. Fax: +92-336-232-1845.
E-mail addresses: ali-waqar.azim@ensimag.grenoble-inp.fr, aliwaqar@ciitwah.edu.pk (A.W. Azim), sabrar@comsats.edu.pk (S. Abrar), azzedine@kfupm.edu.sa (A. Zerguine), asoke.nandi@brunel.ac.uk (A.K. Nandi).

http://dx.doi.org/10.1016/j.dsp.2015.09.002

face and consequently affecting the performance of filters, thus, tracking the variations in underlying signal statistics is considered to be a useful and important property for adaptive filters. These variations in underlying signal statistics and consequently saddle point can be tracked by using *tracking performance analysis*. The performance metric to be considered for tracking performance of an adaptive filter is the steady-state excess mean-square-error (EMSE). The EMSE can be defined as the difference between the mean-square-error (MSE) of the filter in steady-state and its minimum value. The smaller the EMSE of an adaptive filter, the better it is [14]. If filter parameters (like step-size) are chosen correctly, the filter can track variations in underlying signal statistics. However, tracking fast variations might prove to be a challenging task or at times impossible to perform [14].

The widely adopted adaptive blind equalization algorithm is the so-called *Constant Modulus Algorithm* (CMA2–2) [2,15–17]. For quadrature amplitude modulation (QAM) signaling, however, a tailored version of CMA2–2, commonly known as *Multimodulus Algorithm* (MMA2–2) is considered more suitable. The MMA2–2 is capable of jointly achieving blind equalization and carrier phase recovery, whereas the CMA2–2 requires a separate phase-lock loop for achieving carrier phase recovery. The family of MMA, MMAp–q, is associated with the minimization of the dispersion-directed cost-function with two degrees of freedom. By selecting appropriate values of p and q, the generic split cost-function leads to the respective cost-functions of several existing blind equalization algorithms [18–21]. Interested readers are referred to [22] for detailed discussion on MMAp–q. The update expressions of these algorithms are inherently nonlinear in nature due to the presence of nonlinear error-functions [20,23–27].

Algorithms like CMA2–2/MMA2–2 have recently been employed in optical systems for polarization mode demultiplexing and also to mitigate the effects of other types of interferences like chromatic and polarization mode dispersions in optical systems. Since 2008 [28], CMA2–2 and its variants have become the most experimented algorithms for blind polarization demultiplexing [29–36]. In [37], authors have compared CMA2–2 with an independent component analysis (ICA) based algorithm to demultiplex the polarization adaptively. Recently in [38–43], authors have used MMA2–2 and its variants as a joint adaptive solution for blind demultiplexing and carrier phase recovery in coherent optical system. Afterwards, βMMA (which is an optimized version of MMA2–1) [44] has been employed in coherent optical receiver to demultiplex polarization mode signals adaptively [45].

In this paper, the approach that has been adopted for steady-state tracking analysis of multimodulus equalizers exploits the study of energy propagation through each iteration of an adaptive filter using a feedback structure (which consists of a lossless feedforward block and a feedback path), and it relies on energy conservation arguments [14]. The convenience of this approach is that it allows us to avoid working with nonlinear update equations and thus bypasses the need for working directly with the weight error covariance matrix. In particular, using the fundamental variance relation arguments, we derive expressions for steady-state EMSE of MMA2–2, MMA2–1, MMA1–2 and MMA1–1 under the assumption that the quadrature components of the successfully equalized signal are Gaussian distributed when conditioned on true signal alphabets. Our objective is not to study the conditions under which an algorithm will tend to converge successfully, rather to evaluate its expected steady-state performance once it has converged successfully.

1.1. Literature review

The nonlinearity of most of the adaptive equalizers, including CMA2–2 and MMA2–2, makes the steady-state analysis and tracking performance a difficult task to perform. As a result, only a handful of results is available in the literature concerning the steady-state performance of adaptive equalizers. A few results are available on EMSE analysis of CMA2–2 like Fijalkow et al. [46] employed ingenious use of Lyapunov stability and averaging analysis, Shynk et al. [47] used Gaussian regression vector assumption, and some exploited the variance relation theorem [48,49] to evaluate the same. Steady-state analyses of adaptive filters have gained interest due to their ease in analysis. Recently, Abrar et al. [50] performed the EMSE analysis of CMA2–2 and βCMA [51] by assuming that the modulus of equalized signals are Rician distributed in the steady-state. In a recent work [52], we have performed the EMSE analysis of MMA2–2 and βMMA [44] by assuming that the real and imaginary parts of equalized signals are Gaussian distributed in the steady-state. Moreover, the approach of [14] has been employed to study the steady-state performance of a number of adaptive blind equalization algorithms e.g., the so-called hybrid algorithm [53], the square contour algorithm [54], the improved square contour algorithm [55], and the varying-modulus algorithms [56].

1.2. Notation

Unless otherwise mentioned, scalars are represented by italic letters (e.g., K). Lower-case boldface letters are used to denote vectors and upper-case boldface letters are associated with matrices, e.g., $\boldsymbol{w}$ and $\boldsymbol{R}$, respectively. In addition, the symbol $\otimes$ and operators $(\cdot)^*$, $(\cdot)^T$ and $(\cdot)^H$ respectively represents the convolution operation, complex conjugate operator, transpose operator and Hermitian (conjugate transpose) operator. The operator $\|\cdot\|$ when applied to a vector gives the Euclidean norm of the vector, whereas, the operator $|\cdot|$ gives the absolute vector. Further, E, $\Re[\cdot]$ and $\boldsymbol{I}$ denotes the expectation operator, the real part of the complex entity, and identity matrix of appropriate dimensions, respectively. The operator $\mathrm{Tr}(\cdot)$ gives the trace of the matrix.

1.3. Paper organization

The paper is organized as follows: In Section 2, we describe the mathematical model for the system. Section 3 provides a brief introduction of different members of MMA family that we aim to discuss here. Section 4 introduces the non-stationary environment and the framework for EMSE analyses. Section 5 presents the analytical expressions evaluated for steady-state tracking performance analysis for MMA2–2, MMA2–1, MMA1–2 and MMA1–1 equalizers. Section 6 compares the proposed approach with existing state-of-the-art methods. Section 7 provides a number of computer simulations on steady-state tracking performance analysis of the algorithms considering different scenarios: for equalized zero-forcing solution, equalizing a time-varying channel, studying the effect of filter-length on EMSE on a time-invariant channel, and adaptive optical demultiplexing in a coherent optical system. In addition, it also compares the theoretical results predicted by our expressions with the simulated values. Finally, Section 8 draws conclusions.

2. System model

Fig. 1 depicts a typical baseband communication system. Consider that the channel response is given by a K-tap vector $\boldsymbol{h}_n = [h_{n,0}, h_{n,1}, \cdots, h_{n,K-1}]$, then the full rank $(N + K - 1) \times N$ channel convolution matrix $\boldsymbol{\mathcal{H}}$ is given by following Toeplitz matrix

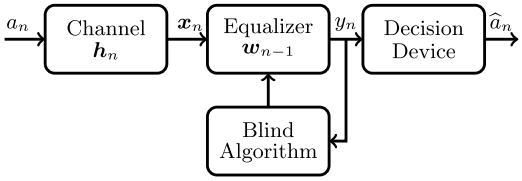

Fig. 1. A typical baseband communication system.

$$\mathcal{H} = \begin{bmatrix} h_{n,0} & 0 & \cdots & 0 & \cdots \\ h_{n,1} & h_{n,0} & \ddots & 0 & \ddots \\ \vdots & h_{n,1} & \ddots & \vdots & \ddots \\ h_{n,K-1} & \vdots & \ddots & h_{n,0} & \ddots \\ 0 & h_{n,K-1} & \ddots & h_{n,1} & \ddots \\ \vdots & \vdots & \cdots & \ddots & \ddots \end{bmatrix} \tag{1}$$

The received signal x_n is the convolution of transmitted sequence $\{a_n\} = [a_n, a_{n-1}, \cdots, a_{n-K+1}]^T$ and channel impulse response $\boldsymbol{h}_n$ as given by $x_n = \boldsymbol{h}_n^T \boldsymbol{a}_n$; the sequence $\{a_n\}$ is independent and identically distributed (i.i.d.), and takes values of equally likely square-QAM symbols. The vector $\boldsymbol{x}_n$ is fed to the equalizer to combat the interference introduced by the propagation channel and estimate delayed version of the transmitted sequence $\{a_{n-\delta}\}$, where δ denotes delay parameter.

Let $\boldsymbol{w}_n = [w_{n,0}, w_{n,1}, \cdots, w_{n,N-1}]^T$ be the impulse response of equalizer and $\boldsymbol{x}_n = [x_n, x_{n-1}, \cdots, x_{n-N+1}]^T$ be the vector of channel observations (the regressor vector) with input covariance matrix $\boldsymbol{R} = \mathrm{E}\boldsymbol{x}_n\boldsymbol{x}_n^H$, where N is the number of equalizer taps. The output of equalizer is the convolution of regression vector and equalizer impulse response is given as $y_n = \boldsymbol{w}_{n-1}^H \boldsymbol{x}_n$. Let $\boldsymbol{t}_n = \boldsymbol{h}_n \otimes \boldsymbol{w}_{n-1}^*$ be the overall channel-equalizer impulse response. Using (1), we obtain $\boldsymbol{t}_n = \boldsymbol{h}_n \otimes \boldsymbol{w}_{n-1}^* = \mathcal{H}\boldsymbol{w}_{n-1}^*$. Under successful convergence, we have $\boldsymbol{t}_n = \boldsymbol{e}$ is ideally single-spike where $\boldsymbol{e} = [0, \cdots, 0, 1, 0, \cdots, 0]^T$.

A generic stochastic gradient-based adaptive equalizer for which the updating algorithm is given as [14]

$$\boldsymbol{w}_n = \boldsymbol{w}_{n-1} + \mu\varphi(y_n)^*\boldsymbol{x}_n \tag{2}$$

where μ is a small positive step-size, governing the speed of convergence and the level of steady-state equalizer performance, and $\varphi(y_n)$ is complex-valued *error function*. For multimodulus equalizers, the error function is non-analytic in nature, i.e., it is a decoupled function of the quadrature components of deconvolved sequence y_n, which is expressed as

$$\varphi(y_n) = \psi(y_{R,n}) + j\psi(y_{I,n}), \tag{3}$$

so that the real and imaginary parts of $\varphi(y_n)$ are obtained from the real $y_{R,n}$ and imaginary parts $y_{I,n}$ of y_n, respectively.

3. The multimodulus equalizers

The *Multimodulus Algorithm* (MMA) is considered more suitable for QAM signaling. A generalized dispersion-directed (split) cost-function of generic MMAp–q equalizers is given as follows [22]:

$$J^{\text{MMA}p-q} = \mathrm{E}\big||y_{R,n}|^p - R_R^p\big|^q + \mathrm{E}\big||y_{I,n}|^p - R_I^p\big|^q \tag{4}$$

where p and q are positive integers, and R_R and R_I are dispersion constants chosen in accordance with the source statistics in order to guarantee that the global minima of $J^{\text{MMA}p-q}$ occurs at zero-forcing solutions. The cost function defined in (4) can be considered as a generalization of *Wesolowski's* cost-function [23] with two degrees of freedom or the split version of Larimore and Treichler (CM) cost-function [57]. The corresponding stochastic gradient-based adaptive algorithm is [22]

$$\begin{aligned}\boldsymbol{w}_n = \boldsymbol{w}_{n-1} + \mu\Big[&\big||y_{R,n}^p| - R_R^p\big|^{q-2}|y_{R,n}^{p-2}|\left(R_R^p - |y_{R,n}^p|\right)y_{R,n} \\ &+ j\big||y_{I,n}^p| - R_I^p\big|^{q-2}|y_{I,n}^{p-2}|\left(R_I^p - |y_{I,n}^p|\right)y_{I,n}\Big]^*\boldsymbol{x}_n\end{aligned} \tag{5}$$

A multitude of algorithms can be obtained for different choices of p and q, providing a possible flexibility in the design of blind equalizers. In the sequel, the algorithm defined by recursion (5) is referred as MMAp–q and for the sake of simplicity, we will use subscript L to denote either R or I. Expression (5) generalizes a number of existing blind adaptive equalization algorithms. Among them, these are the following:

1. For $p = q = 2$, (4) reduces to following split cost function which was proposed independently by Wesolowski [19], Oh and Chin [20] and Yang et al. [24]:

$$J^{\text{MMA2–2}} = \min_{\boldsymbol{w}}\left\{\mathrm{E}\left(y_{R,n}^2 - R_R^2\right)^2 + \mathrm{E}\left(y_{I,n}^2 - R_I^2\right)^2\right\} \tag{6}$$

where $R_L^2 = \mathrm{E}a_L^4/\mathrm{E}a_L^2$. The tap weight vector of MMA2–2 is updated according to

$$\boldsymbol{w}_n = \boldsymbol{w}_{n-1} + \mu\left[(R_R^2 - y_{R,n}^2)y_{R,n} + j(R_I^2 - y_{I,n}^2)y_{I,n}\right]^*\boldsymbol{x}_n \tag{7}$$

2. For $p = 2$ and $q = 1$, (4) results in MMA2–1 equalization algorithm that employs the following cost function[1]

$$J^{\text{MMA2–1}} = \min_{\boldsymbol{w}}\left\{\mathrm{E}\left|y_{R,n}^2 - R_R^2\right| + \mathrm{E}\left|y_{I,n}^2 - R_I^2\right|\right\} \tag{8}$$

The tap weight vector of MMA2–1 is updated to minimize (8) using a gradient-descent adjustment algorithm according to

$$\begin{aligned}\boldsymbol{w}_n = \boldsymbol{w}_{n-1} + \mu\big[&\mathrm{sgn}\big(R_R^2 - y_{R,n}^2\big)y_{R,n} \\ &+ j\,\mathrm{sgn}\big(R_I^2 - y_{I,n}^2\big)y_{I,n}\big]^*\boldsymbol{x}_n\end{aligned} \tag{9}$$

3. For $p = 1$, $q = 2$, (4) reduces to an equivalent form of Benveniste–Goursat cost–function [18]. We denote the resulting algorithm as MMA1–2, and ultimately (4) results in

$$J^{\text{MMA1–2}} = \min_{\boldsymbol{w}}\left\{\mathrm{E}\left(|y_{R,n}| - R_R\right)^2 + \mathrm{E}\left(|y_{I,n}| - R_I\right)^2\right\} \tag{10}$$

where $R_L = \mathrm{E}a_L^2/\mathrm{E}|a_L|$. The tap weight vector of MMA1–2 is updated to minimize (10) using a gradient-descent adjustment algorithm according to

$$\begin{aligned}\boldsymbol{w}_n = \boldsymbol{w}_{n-1} + \mu\big[&\big(R_R\ \mathrm{sgn}(y_{R,n}) - y_{R,n}\big) \\ &+ j\big(R_I\ \mathrm{sgn}\,(y_{I,n}) - y_{I,n}\big)\big]^*\boldsymbol{x}_n\end{aligned} \tag{11}$$

4. For $p = q = 1$, (4) reduces to an equivalent form of the cost-function independently proposed by Weerackody et al. in 1991 [58] and Im et al. in 2001 [21]. We denote the resulting algorithm as MMA1–1 and its cost function is given as follows[2]:

[1] In MMA2–1, the dispersion constant R_L is obtained as $R_L = 2\lceil z\rceil - 1$, where $\lceil z\rceil$ is the smallest positive integer greater than or equal to z [22]. The parameter z is given by $z = (z_1/12) + (1/z_1)$ where z_1 is given as $\sqrt[3]{108z_2 + 12\sqrt{81z_2^2 - 12}}$, $z_2 = 0.5\sqrt{M}(M-1)$ and M denotes the size of constellation. It gives R_L = 3, 7, and 13 for 16-, 64-, and 256-QAM, respectively.

[2] The dispersion constant R_L for MMA1–1 is given as $R_L = 2\lceil z\rceil - 1$ [22]. For M-point constellation we have $z = \sqrt{M/8}$ which gives $R_L = 3, 5,$ and 11 for 16-, 64-, and 256-QAM, respectively.

$$J^{\text{MMA1-1}} = \min_{\boldsymbol{w}} \left\{ \mathrm{E}\big||y_{R,n}| - R_R\big| + \mathrm{E}\big||y_{I,n}| - R_I\big| \right\} \tag{12}$$

The tap weight vector of MMA1–1 is updated to minimize (12) using a gradient-descent adjustment algorithm according to

$$\begin{aligned} \boldsymbol{w}_n = \boldsymbol{w}_{n-1} + \mu \big[& \operatorname{sgn}\left(R_R \operatorname{sgn}(y_{R,n}) - y_{R,n}\right) \\ & + j \operatorname{sgn}\left(R_I \operatorname{sgn}(y_{I,n}) - y_{I,n}\right) \big]^* \boldsymbol{x}_n \end{aligned} \tag{13}$$

4. Non-stationary environment and energy conservation relation

We consider a non-stationary system model in which the variations in the Wiener solution, $\boldsymbol{w}^o$, follow usually a first-order random walk model [14]:

$$\boldsymbol{w}_n^o = \boldsymbol{w}_{n-1}^o + \boldsymbol{q}_n \tag{14}$$

where the random vector $\boldsymbol{q}_n$ is an i.i.d. zero-mean random vector with positive definite covariance matrix given as $\boldsymbol{Q} = \mathrm{E}\boldsymbol{q}_n\boldsymbol{q}_n^H = \sigma_q^2\boldsymbol{I}$. We assume that $\boldsymbol{q}_n$ is independent of both $\{a_m\}$ and $\{\boldsymbol{x}_m, \boldsymbol{w}_{-1}^o\}$ for all $m < n$ [14]. Using the time-dependent Wiener solution, the desired data a_n can be expressed as

$$a_n = (\boldsymbol{w}_{n-1}^o)^H \boldsymbol{x}_n + \vartheta_n, \tag{15}$$

where ϑ_n is the measurement or gradient noise and is uncorrelated with $\boldsymbol{x}_n$, i.e., $\mathrm{E}\vartheta_n^*\boldsymbol{x}_n = 0$ [59]. Defining the weight error vector $\tilde{\boldsymbol{w}}_n$ as $\tilde{\boldsymbol{w}}_n := \boldsymbol{w}_n^o - \boldsymbol{w}_n$, (2), for a non-stationary environment is expressed as

$$\tilde{\boldsymbol{w}}_n = \tilde{\boldsymbol{w}}_{n-1} - \mu\varphi(y_n)^*\boldsymbol{x}_n + \boldsymbol{q}_n \tag{16}$$

Defining the so-called *a priori* and *a posteriori* estimation errors as $e_{a,n} := \tilde{\boldsymbol{w}}_{n-1}^H\boldsymbol{x}_n$ and $e_{p,n} := (\tilde{\boldsymbol{w}}_n - \boldsymbol{q}_n)^H\boldsymbol{x}_n$, respectively. We can rewrite (16) in terms of the error measures $\{\tilde{\boldsymbol{w}}_n, \tilde{\boldsymbol{w}}_{n-1}, e_{a,n}, e_{p,n}\}$ alone. For this purpose, we note that if we multiply (16) by $\boldsymbol{x}_n$ from the right, we find that the *a priori* and *a posteriori* estimation errors $\{e_{a,n}, e_{p,n}\}$ are related via

$$e_{a,n} = e_{p,n} + \mu\|\boldsymbol{x}_n\|^2\varphi(y_n) \tag{17}$$

Relation (17) reveals that $e_{a,n}$ depends on channel variation, adaption, and gradient noise. Thus, the steady-state EMSE and the tracking performance of an adaptive equalizer can be quantified by the energy of $e_{a,n}$. From (17), we can associate the error-function of an equalizer with the *a priori* and the *a posteriori* estimation errors as follows:

$$\varphi(y_n) = \frac{e_{a,n} - e_{p,n}}{\mu\|\boldsymbol{x}_n\|^2} \tag{18}$$

Substituting (18) in (16) and rearranging the terms, we obtain the energy conservation relation

$$\|\tilde{\boldsymbol{w}}_n\|^2 + \frac{|e_{a,n}|^2}{\|\boldsymbol{x}_n\|^2} = \|\tilde{\boldsymbol{w}}_{n-1}\|^2 + \frac{|e_{p,n}|^2}{\|\boldsymbol{x}_n\|^2} \tag{19}$$

It is important to note that (19) holds for any adaptive algorithm. Fig. 2 represents the physical interpretation of (19) which links the energies of the weight error vector as well as the *a priori* and the *a posteriori* estimation errors by stating that mapping from the variables $\left\{\tilde{\boldsymbol{w}}_{n-1}, e_{p,n}/\|\boldsymbol{x}_n\|\right\}$ to the variables $\left\{\tilde{\boldsymbol{w}}_n, e_{a,n}/\|\boldsymbol{x}_n\|\right\}$ is energy preserving. The relation (19) characterizes the energy preserving property of the feed-forward path, whereas the relation (17) characterizes the feedback path. The function $\mathcal{M}$ denotes the mapping between the two variables and z^{-1} denotes the unit delay operator. Substituting the expression of $e_{p,n}$ from (17) into (19), we get the fundamental variance relation theorem.

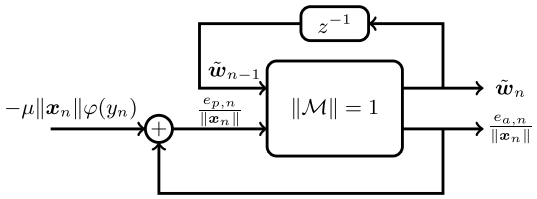

Fig. 2. Lossless mapping and feedback loop.

Theorem 1 *(Variance relation). (See [14].) Consider any adaptive filter of the form (2), and assume filter operation in steady-state. Assume further that* $a_n = (\boldsymbol{w}_{n-1}^o)^H\boldsymbol{x}_n + \vartheta_n$, *where* $\boldsymbol{w}_{n-1}^o$ *varies according to the random-walk model (14), where* $\boldsymbol{q}_n$ *is a zero-mean i.i.d. sequence with covariance matrix* $\boldsymbol{Q}$. *Moreover,* $\boldsymbol{q}_n$ *is independent of* $\{a_m\}$ *and* $\{\boldsymbol{x}_m, \boldsymbol{w}_{-1}^o\}$ *for all* $m < n$. *With* $y_n = a_n - e_{a,n}$, *it is true that*

$$2\mathrm{E}\Re\left[e_{a,n}^*\varphi(y_n)\right] = \mu\mathrm{Tr}(\boldsymbol{R})\mathrm{E}|\varphi(y_n)|^2 + \mu^{-1}\mathrm{Tr}(\boldsymbol{Q}) \tag{T1.1}$$

Expression (T1.1) can be solved for steady-state EMSE, which is defined as

$$\text{EMSE} \triangleq \lim_{n\to\infty} \mathrm{E}|e_{a,n}|^2 \tag{20}$$

The procedure of evaluating EMSE using (T1.1) avoids the need for explicit evaluation of $\mathrm{E}\|\tilde{\boldsymbol{w}}_n\|^2$ or its steady-state value $\mathrm{E}\|\tilde{\boldsymbol{w}}_\infty\|^2$ which can be a burden especially for adaptive schemes with nonlinear update equations. In the sequel, in addition to the variance relation, the following justified assumptions are used:

- **A1)** In steady-state the *a priori* estimation error $e_{a,n}$ is independent of both the transmitted sequence $\{a_n\}$ and the regressor vector $\boldsymbol{x}_n$ [14].
- **A2)** The number of filter taps is large enough so that by virtue of the central limit theorem, $e_{a,n}$ is zero-mean complex valued Gaussian [59,60].
- **A3)** The optimum filter achieves perfect equalization (zero-forcing solution) $a_n \approx (\boldsymbol{w}_{n-1}^o)^H\boldsymbol{x}_n$; however, due to channel variation and gradient noise, the equalizer weight vector is not equal to $\boldsymbol{w}_n^o$ even in steady-state [61]. Additionally, no additive noise is assumed in the system (see [48,49,62–67]).

Assumption **A1** is the orthogonality condition required for a successful convergence. Assumption **A2**, the Gaussianity of *a priori* estimation error, has appeared in a number of recent publications. For example, Bellini [68] discussed that the convolutional noise (which bears similar mathematical definition as that of *a priori* estimation error) may be considered as zero-mean Gaussian. Moreover, [69] discussed that the *a priori* estimation error (for a long equalizer) may be modeled as a zero-mean Gaussian random variable. It has been shown that the steady-state *a priori* estimation error is zero-mean Gaussian, even for the case where the measurement noise is taken to be uniformly distributed. The assumption **A3** is based on the understanding that CMA2–2 and similarly its multimodulus variants diverge on infinite time horizon when noise is unbounded. Interested readers may refer to [70] for a detailed discussion on this issue. Note that the (total) mean square error, MSE of a non-diverging equalizer in the presence of additive noise, however, can always be given as $\text{MSE} = \sigma_\vartheta^2 + \text{EMSE}$, where σ_ϑ^2 is the variance of modeling error/measurement noise. The degree of non-stationarity (DN) of the data is defined as $\text{DN} \triangleq \sqrt{\mathrm{Tr}(\boldsymbol{R}\boldsymbol{Q})/\sigma_\vartheta^2}$ [14]. $\text{DN} > 1$ means that the statistical variations in the optimal weight vector are too fast for the filter to track them. However, if $\text{DN} \ll 1$, then the filter would generally be able to track the variations in weight vector [14].

Here onwards, for the sake of notational simplicity, we use $\zeta := \text{EMSE}$, $e_a := e_{a,n}$, $y := y_n$, $a := a_n$, $\varphi := \varphi(y_n)$ and $P_a = \mathrm{E}|a|^2 = \mathrm{E}(a_R^2 + a_I^2)$. Also, the acronyms LHS and RHS are used to denote the left-hand side and the right-hand side, respectively.

5. Steady-state EMSE analysis

We now apply the fundamental variance relation to different MMA adaptive algorithms to obtain analytical expressions for steady-state EMSE by evaluating the energy of error-function as well as its correlation with *a priori* estimation error. Due to space limitations, we omit some trivial details and only highlight the main steps in the arguments.

5.1. The EMSE of MMA2–2 equalizer

Using the fundamental variance relation (T1.1), we have the following theorem for the tracking EMSE of MMA2–2 equalizer:

Theorem 2 *(Tracking EMSE of MMA2–2). Consider the MMA2–2 recursion (7) with complex-valued data. Consider the non-stationary model (14) with a sufficiently small degree of non-stationarity. Then its EMSE can be approximated by the following expression for a sufficiently small step-size μ:*

$$\zeta^{\text{MMA2–2}}(\mu) = \frac{\mu c_1 + \frac{1}{\mu}\mathrm{Tr}(\boldsymbol{Q})}{c_2 - \mu c_3}, \tag{T2.1}$$

$$\mu_{\text{opt}}^{\text{MMA2–2}} = \frac{\sqrt{\mathrm{Tr}(\boldsymbol{Q})c_1c_2^2 + \mathrm{Tr}(\boldsymbol{Q})^2c_3^2} - \mathrm{Tr}(\boldsymbol{Q})c_3}{c_1c_2}$$
$$\text{with } \zeta_{\min}^{\text{MMA2–2}} = \frac{2\mathrm{Tr}(\boldsymbol{Q})}{\mu_{\text{opt}}c_2} \tag{T2.2}$$

where, $c_1 := 2\mathrm{Tr}(\boldsymbol{R})\big(\mathrm{E}a_R^6 - 2R_R^2\mathrm{E}a_R^4 + R_R^4\mathrm{E}a_R^2\big)$, $c_2 := 2(3\mathrm{E}a_R^2 - R_R^2)$, and $c_3 := \mathrm{Tr}(\boldsymbol{R})\big(3\mathrm{E}a_R^4 + R_R^4\big)$. Substituting the expression for μ_{opt} into the expression of EMSE we find the corresponding optimal EMSE.

Proof. In [52], we obtained the following polynomial for EMSE of MMA2–2:

$$\begin{aligned}&\tfrac{15}{4}\zeta^3\mu\mathrm{Tr}(\boldsymbol{R}) + \zeta^2\left(\mu\mathrm{Tr}(\boldsymbol{R})\left(\tfrac{45}{2}\mathrm{E}a_R^2 - 3R_R^2\right) - 3\right)\\ &- \zeta\left(6\mathrm{E}a_R^2 - 2R_R^2 - \mu\mathrm{Tr}(\boldsymbol{R})\left(3\mathrm{E}a_R^4 + R_R^4\right)\right)\\ &+ \mu\mathrm{Tr}(\boldsymbol{R})\left(2\mathrm{E}a_R^6 + 2R_R^4\mathrm{E}a_R^2 - 4R_R^2\mathrm{E}a_R^4\right)\\ &+ \mu^{-1}\mathrm{Tr}(\boldsymbol{Q}) = 0\end{aligned} \tag{21}$$

In order to evaluate some closed-form expressions of $\zeta^{\text{MMA2–2}}$, certain approximations have to be made, e.g., by neglecting the cubic and quadratic terms in (21), we obtain

$$\begin{aligned}&\zeta\left(\mu\mathrm{Tr}(\boldsymbol{R})(3\mathrm{E}a_R^4 + R_R^4) - 6\mathrm{E}a_R^2 + 2R_R^2\right)\\ &+ \mu\mathrm{Tr}(\boldsymbol{R})\left(2\mathrm{E}a_R^6 + 2R_R^4\mathrm{E}a_R^2 - 4R_R^2\mathrm{E}a_R^4\right)\\ &+ \mu^{-1}\mathrm{Tr}(\boldsymbol{Q}) = 0\end{aligned} \tag{22}$$

which yields the following closed-form solution:

$$\zeta^{\text{MMA2–2}} = \frac{\mu^2\mathrm{Tr}(\boldsymbol{R})\left(2\mathrm{E}a_R^6 + 2R_R^4\mathrm{E}a_R^2 - 4R_R^2\mathrm{E}a_R^4\right) + \mathrm{Tr}(\boldsymbol{Q})}{\mu(6\mathrm{E}a_R^2 - 2R_R^2) - \mu^2\mathrm{Tr}(\boldsymbol{R})(3\mathrm{E}a_R^4 + R_R^4)} \tag{23}$$

□

5.2. The EMSE of MMA2–1 equalizer

Under similar conditions and assumptions, as mentioned in Section 4, we have following theorem for MMA2–1:

Theorem 3 *(Tracking EMSE of MMA2–1). Consider the MMA2–1 recursion (9) with complex-valued data. Consider the non-stationary model (14) with a sufficiently small degree of non-stationarity. Then its EMSE can be approximated by the following expression for a sufficiently small step-size μ:*

$$\zeta^{\text{MMA2–1}}(\mu) = \left(\frac{-c_3 + \sqrt{c_3^2 + 4(c_1 - c_2\mu)(P_ac_2\mu + \frac{1}{\mu}\mathrm{Tr}(\boldsymbol{Q}))}}{2(c_1 - c_2\mu)}\right)^2, \tag{T3.1}$$

$$\mu_{\text{opt}}^{\text{MMA2–1}} = \sqrt{\frac{\mathrm{Tr}(\boldsymbol{Q})}{\mathrm{Tr}(\boldsymbol{R})P_a}} \quad \text{with } \zeta_{\min}^{\text{MMA2–1}} = \zeta^{\text{MMA2–1}}\left(\mu_{\text{opt}}^{\text{MMA2–1}}\right), \tag{T3.2}$$

where $c_1 := 2(\frac{2}{\sqrt{M}} - 1)$, $c_2 := \mathrm{Tr}(\boldsymbol{R})$, $c_3 := \frac{8R_R}{\sqrt{\pi M}}$, and M is the size of square-QAM. Substituting the expression for μ_{opt} into the expression of EMSE we find the corresponding optimal EMSE.

Proof. For MMA2–1 equalizer, the error-function is given as $\varphi = f_Ry_R + jf_Iy_I = \varphi_R + j\varphi_I$. For simplicity we can represent the real and imaginary parts of the error-function as φ_L, where φ_L is equal to y_L and $-y_L$ for $|y_{L,n}| < R_L$ and $|y_{L,n}| > R_L$, respectively. We obtain $\mathrm{E}|\varphi|^2$ for MMA2–1 as follows:

$$\begin{aligned}\mathrm{E}|\varphi|^2 &= \mathrm{E}\left[y_{R\{|y_R|<R_R\}}^2 + y_{R\{|y_R|>R_R\}}^2 + y_{I\{|y_I|<R_I\}}^2 + y_{R\{|y_I|>R_I\}}^2\right]\\ &= \mathrm{E}\left[y_R^2 + y_I^2\right] = \mathrm{E}y_R^2 + \mathrm{E}y_I^2\end{aligned} \tag{24}$$

Substituting $\mathrm{E}y_L^2$, it follows immediately that $\mathrm{E}|\varphi|^2 = P_a + \zeta$. Thus the RHS of (T1.1) for MMA2–1 is thus evaluated as follows:

$$\mathrm{RHS} = \mu\mathrm{Tr}(\boldsymbol{R})\,(P_a + \zeta) + \mu^{-1}\mathrm{Tr}(\boldsymbol{Q}) \tag{25}$$

Next substituting the *a priori* error in (T1.1), and computing the correlation between equalizer error-function and conjugate of *a priori* error, the LHS of (T1.1) for MMA2–1 is evaluated as:

$$\begin{aligned}\mathrm{LHS} &= 2\mathrm{E}\Re\left[e_a^*\varphi\right]\\ &= 2\mathrm{E}\Big[a_Rf_Ry_R - f_Ry_R^2 + a_If_Iy_I - f_Iy_I^2\Big]\\ &= 2\mathrm{E}\Big[\left(a_Ry_R - y_R^2\right)_{\{|y_R|<R_R\}} - \left(a_Ry_R - y_R^2\right)_{\{|y_R|>R_R\}}\\ &\quad + \left(a_Iy_I - y_I^2\right)_{\{|y_I|<R_I\}} - \left(a_Iy_I - y_I^2\right)_{\{|y_I|>R_I\}}\Big]\\ &= 2\mathrm{E}\left(a_Ry_R - y_R^2\right) - 8\mathrm{E}\left(a_Ry_R - y_R^2\right)_{\{y_R>R_R\}}\\ &\quad + 2\mathrm{E}\left(a_Iy_I - y_I^2\right) - 8\mathrm{E}\left(a_Iy_I - y_I^2\right)_{\{y_I>R_I\}}\end{aligned} \tag{26}$$

Exploiting assumption **A2**, we obtain

$$\begin{aligned}\mathrm{LHS} &= -2\zeta + 8\mathrm{E}\left[\frac{R_R}{2}\sqrt{\frac{\zeta}{\pi}}\exp\left(-\frac{(a_R - R_R)^2}{\zeta}\right)\right.\\ &\quad \left.+ \frac{\zeta}{4}\left(1 + \mathrm{erf}\left(\frac{a_R - R_R}{\sqrt{\zeta}}\right)\right)\right]\\ &\quad + 8\mathrm{E}\left[\frac{R_I}{2}\sqrt{\frac{\zeta}{\pi}}\exp\left(-\frac{(a_I - R_I)^2}{\zeta}\right)\right.\\ &\quad \left.+ \frac{\zeta}{4}\left(1 + \mathrm{erf}\left(\frac{a_I - R_I}{\sqrt{\zeta}}\right)\right)\right]\end{aligned} \tag{27}$$

where erf(·), the *Gauss error function*, is defined as $\mathrm{erf}(x) = \frac{2}{\sqrt{\pi}}\int_0^x \exp\left(-t^2\right) \mathrm{d}t$. Owing to four quadrant symmetry of QAM constellation, the moments evaluated for in-phase component are same as those for quadrature component. Simplifying and combining (25) and (27), we obtain

$$-2\zeta + A - \mu \mathrm{Tr}(\boldsymbol{R})\,(P_a + \zeta) - \mu^{-1}\mathrm{Tr}(\boldsymbol{Q}) = 0 \tag{28}$$

where $A := 16\mathrm{E}\big[\frac{R_R}{2}\sqrt{\frac{\zeta}{\pi}}\exp\big(-\frac{(a_R - R_R)^2}{\zeta}\big) + \frac{\zeta}{4}(1 + \mathrm{erf}(\frac{a_R - R_R}{\sqrt{\zeta}}))\big]$. Since the argument inside the exponent function, $(a_R - R_R)^2$, is always positive, we have $\exp(\cdot) = 0$ for $a_R \neq R_R$ and $\zeta \ll 1$. However, when $a_R = R_R$, we have $\exp(\cdot) = 1$ with probability $\mathrm{P_r}[a_R = R_R]$. Similarly, under the assumption $\zeta \ll 1$, erf(·) is equal to -1, and 0, respectively, for the cases $(a_R < R_R)$, and $(a_R = R_R)$. These considerations yield

$$A \approx \begin{cases} 0, & \text{if } a_R \neq R_R \\ \left(8R_R\sqrt{\frac{\zeta}{\pi}} + 4\zeta\right)\mathrm{P_r}[a_R = R_R], & \text{if } a_R = R_R \end{cases} \tag{29}$$

Since an M-point constellation is being considered, the probability $\mathrm{P_r}[a_R = R_R]$ is equal to $1/\sqrt{M}$. Denoting $c_1 := 2(\frac{2}{\sqrt{M}} - 1)$, $c_2 := \mathrm{Tr}(\boldsymbol{R})$, $c_3 := \frac{8R_R}{\sqrt{\pi M}}$, and $c_4 := \mathrm{Tr}(\boldsymbol{R})P_a$, and by combining (28)–(29), we obtain

$$(c_1 - c_2\mu)\zeta + c_3\sqrt{\zeta} - (c_4\mu + \tfrac{1}{\mu}\mathrm{Tr}(\boldsymbol{Q})) = 0. \tag{30}$$

Solving it by quadratic formula we obtain (T3.1). Further, substituting $\zeta = v^2$ and taking derivative with respect to μ, we obtain $(2vc_1 + c_3)\frac{\mathrm{d}v}{\mathrm{d}\mu} - v^2c_2 - c_4 + \mu^{-2}\mathrm{Tr}(\boldsymbol{Q}) = 0$. For the optimum value of μ, we have $\frac{\mathrm{d}v}{\mathrm{d}\mu} = 0$; this gives

$$\mu_{\mathrm{opt}}^{\mathrm{MMA2\text{-}1}} = \sqrt{\frac{\mathrm{Tr}(\boldsymbol{Q})}{c_4 + c_2\zeta_{\mathrm{min}}^{\mathrm{MMA2\text{-}1}}}} \tag{31}$$

Since $c_2\zeta_{\mathrm{min}}^{\mathrm{MMA2\text{-}1}} \ll c_4$, thus ignoring it we obtain (T3.2). □

5.3. The EMSE of MMA1–2 equalizer

Under similar conditions and assumptions, as mentioned in Section 4, we have following theorem for MMA1–2:

Theorem 4 *(Tracking EMSE of MMA1–2). Consider the MMA1–2 recursion (11) with complex-valued data. Consider the non-stationary model (14) with a sufficiently small degree of non-stationarity. Then its EMSE can be approximated by the following expression for a sufficiently small step-size μ:*

$$\zeta^{\mathrm{MMA1\text{-}2}}(\mu) = \frac{\mu c_1 + \frac{1}{\mu}\mathrm{Tr}(\boldsymbol{Q})}{2 - \mu\,\mathrm{Tr}(\boldsymbol{R})}, \tag{T4.1}$$

$$\mu_{\mathrm{opt}}^{\mathrm{MMA1\text{-}2}} = \sqrt{\frac{\mathrm{Tr}(\boldsymbol{Q})}{c_1}} \quad \textit{with } \zeta_{\mathrm{min}}^{\mathrm{MMA1\text{-}2}} = \zeta^{\mathrm{MMA1\text{-}2}}\left(\mu_{\mathrm{opt}}^{\mathrm{MMA1\text{-}2}}\right), \tag{T4.2}$$

where $c_1 := 2\,\mathrm{Tr}(\boldsymbol{R})\,\mathrm{E}(R_R - |a_R|)^2$. Substituting the expression for μ_{opt} into the expression of EMSE we find the corresponding optimal EMSE.

Proof. For MMA1–2 equalizer, we have $\varphi = \varphi_R + j\varphi_I$, where φ_L is equal to $(R_L - y_L)$ and $(-R_L - y_L)$ for $y_L > 0$ and $y_L < 0$, respectively. Now, substituting the error-function in (T1.1) and then plugging in the required moments, it follows immediately that

$$\begin{aligned}
\mathrm{E}|\varphi|^2 &= \mathrm{E}\left[(R_R\,\mathrm{sgn}(y_R) - y_R)^2 + (R_I\,\mathrm{sgn}(y_I) - y_I)^2\right] \\
&= \mathrm{E}\left[R_R^2 + y_R^2 - 2R_R|y_R| + R_I^2 + y_I^2 - 2R_I|y_I|\right] \\
&= R_R^2 + \mathrm{E}y_R^2 - 2R_R\mathrm{E}|y_R| + R_I^2 + \mathrm{E}y_I^2 - 2R_I\mathrm{E}|y_I| \\
&= R_R^2 + P_a + \zeta - 2R_R\mathrm{E}\left[\exp\left(-\frac{a_R^2}{\zeta}\right)\sqrt{\frac{\zeta}{\pi}} + a_R\mathrm{erf}\left(\frac{a_R}{\sqrt{\zeta}}\right)\right] \\
&\quad + R_I^2 - 2R_I\mathrm{E}\left[\exp\left(-\frac{a_I^2}{\zeta}\right)\sqrt{\frac{\zeta}{\pi}} + a_I\mathrm{erf}\left(\frac{a_I}{\sqrt{\zeta}}\right)\right]
\end{aligned} \tag{32}$$

Using (32), the RHS for MMA1–2 equalizer becomes:

$$\begin{aligned}
\mathrm{RHS} = \mu\mathrm{Tr}(\boldsymbol{R})\Bigg(&R_R^2 + P_a + \zeta \\
&- 2R_R\mathrm{E}\left[\exp\left(-\frac{a_R^2}{\zeta}\right)\sqrt{\frac{\zeta}{\pi}} + a_R\mathrm{erf}\left(\frac{a_R}{\sqrt{\zeta}}\right)\right] \\
&+ R_I^2 - 2R_I\mathrm{E}\left[\exp\left(-\frac{a_I^2}{\zeta}\right)\sqrt{\frac{\zeta}{\pi}} + a_I\mathrm{erf}\left(\frac{a_I}{\sqrt{\zeta}}\right)\right]\Bigg) \\
&+ \mu^{-1}\mathrm{Tr}(\boldsymbol{Q})
\end{aligned} \tag{33}$$

The LHS of (T1.1) for MMA1–2 can be evaluated as:

$$\begin{aligned}
\mathrm{LHS} &= 2\mathrm{E}\Re\left[e_a^*\varphi\right] \\
&= 2R_R\mathrm{E}\left(a_R\,\mathrm{sgn}(y_R)\right) - 2\mathrm{E}\left(a_R y_R\right) - 2R_R\mathrm{E}|y_R| + 2\mathrm{E}y_R^2 \\
&\quad + 2R_I\mathrm{E}\left(a_I\,\mathrm{sgn}(y_I)\right) - 2\mathrm{E}\left(a_I y_I\right) - 2R_I\mathrm{E}|y_I| + 2\mathrm{E}y_I^2
\end{aligned} \tag{34}$$

Exploiting assumption **A2** and after some straightforward mathematical manipulation, it follows that

$$\begin{aligned}
\mathrm{LHS} = 2\zeta &- 2R_R\mathrm{E}\left[\exp\left(-\frac{a_R^2}{\zeta}\right)\sqrt{\frac{\zeta}{2}}\right] \\
&- 2R_I\mathrm{E}\left[\exp\left(-\frac{a_I^2}{\zeta}\right)\sqrt{\frac{\zeta}{2}}\right]
\end{aligned} \tag{35}$$

Owing to four quadrant symmetry of QAM constellation, the moments evaluated for in-phase component are same as those for quadrature component. Simplifying the equality LHS = RHS, we obtain

$$\begin{aligned}
&2\zeta - 4R_R A - \mu\mathrm{Tr}(\boldsymbol{R})\left(2R_R^2 + P_a + \zeta - 4R_R B\right) \\
&-\mu^{-1}\mathrm{Tr}(\boldsymbol{Q}) = 0
\end{aligned} \tag{36}$$

where $A := \mathrm{E}[\exp\left(-\frac{a_R^2}{\zeta}\right)\sqrt{\frac{\zeta}{2}}]$ and $B := \mathrm{E}\big[\exp\left(-\frac{a_R^2}{\zeta}\right)\sqrt{\frac{\zeta}{\pi}} + a_R\mathrm{erf}(\frac{a_R}{\sqrt{\zeta}})\big]$. Since the argument inside the exponent function, a_R^2, is always positive, and $\zeta \ll 1$, thus we have $\exp(\cdot) = 0$ for both $(a_R > 0)$, and $(a_R < 0)$. Similarly, under the assumption $\zeta \ll 1$, erf(·) is equal to $+1$ and -1, respectively, for the cases $(a_R > 0)$, and $(a_R < 0)$. These considerations yield $A \approx 0$ and $B \approx \mathrm{E}|a_R|$. So, we can rewrite the equality in (36) as

$$2\zeta - 2\mu\mathrm{Tr}(\boldsymbol{R})\left(\tfrac{\zeta}{2} + \mathrm{E}(R_R - |a_R|)^2\right) - \mu^{-1}\mathrm{Tr}(\boldsymbol{Q}) = 0 \tag{37}$$

Solving (37) for ζ, we directly obtain

$$\zeta^{\mathrm{MMA1\text{-}2}} = \frac{2\mu\mathrm{Tr}(\boldsymbol{R})\mathrm{E}(R_R - |a_R|)^2 + \mu^{-1}\mathrm{Tr}(\boldsymbol{Q})}{2 - \mu\mathrm{Tr}(\boldsymbol{R})} \tag{38}$$

Denoting $c_1 := 2\mathrm{Tr}(\boldsymbol{R})\mathrm{E}(R_R - |a_R|)^2$, and $c_2 := \mathrm{Tr}(\boldsymbol{R})$ we obtain (T4.1). Further, substituting $\zeta = v^2$ and taking derivative with respect to μ, we obtain $2v\frac{\mathrm{d}v}{\mathrm{d}\mu} - v^2c_2 - c_1 + \mu^{-2}\mathrm{Tr}(\boldsymbol{Q}) = 0$. For the optimum value of μ, we have $\frac{\mathrm{d}v}{\mathrm{d}\mu} = 0$; this gives

$$\mu_{\text{opt}}^{\text{MMA1-2}} = \sqrt{\frac{\text{Tr}(\boldsymbol{Q})}{c_1 + c_2\zeta_{\min}^{\text{MMA1-2}}}} \tag{39}$$

We can assume that the term $c_2\zeta_{\min}^{\text{MMA2-1}}$ is negligible relative to the first term c_1, thus ignoring it we obtain (T4.2). □

5.4. The EMSE of MMA1–1 equalizer

Under similar conditions and assumptions, as discussed earlier, we have the following theorem for MMA1–1:

Theorem 5 *(Tracking EMSE of MMA1–1). Consider the MMA1–1 recursion (13) with complex-valued data. Consider the non-stationary model (14) with a sufficiently small degree of non-stationarity. Then its EMSE can be approximated by the following expression for a sufficiently small step-size μ:*

$$\zeta^{\text{MMA1-1}}(\mu) = \left(\frac{2\text{Tr}(\boldsymbol{R})\mu + \frac{1}{\mu}\text{Tr}(\boldsymbol{Q})}{(8/\sqrt{M\pi})}\right)^2, \tag{T5.1}$$

$$\mu_{\text{opt}}^{\text{MMA1-1}} = \sqrt{\frac{\text{Tr}(\boldsymbol{Q})}{2\text{Tr}(\boldsymbol{R})}} \quad \textit{with} \quad \zeta_{\min}^{\text{MMA1-1}} = \zeta^{\text{MMA1-1}}\left(\mu_{\text{opt}}^{\text{MMA1-1}}\right). \tag{T5.2}$$

Substituting the expression for μ_{opt} into the expression of EMSE we find the corresponding optimal EMSE.

Proof. For the MMA1–1 equalizer, we have $\varphi_n = \varphi_R + j\varphi_I$, where φ_L is equal to $+1$ for $|y_L| < R_L$ and -1 for $|y_L| > R_L$. Now, substituting the error-function in (T1.1), the energy of the error-function $\text{E}|\varphi|^2$ as follows:

$$\begin{aligned}\text{E}|\varphi|^2 &= \text{E}\big[(+1)^2_{\{|y_R|<R_R\}} + (-1)^2_{\{|y_R|>R_R\}} \\ &\quad + (+1)^2_{\{|y_I|<R_I\}} + (-1)^2_{\{|y_I|>R_I\}}\big] \\ &= \text{E}\left[1_{\{-\infty<y_R<\infty\}} + 1_{\{-\infty<y_I<\infty\}}\right] = 2\end{aligned} \tag{40}$$

After the evaluation of $\text{E}|\varphi|^2$, it immediately follows that

$$\text{RHS} = 2\mu\text{Tr}(\boldsymbol{R}) + \mu^{-1}\text{Tr}(\boldsymbol{Q}) \tag{41}$$

Substituting the conjugate *a priori* estimation error $e_{a,n}^*$ in (T1.1), we can obtain the LHS of (T1.1) for MMA1–1 equalizer as follows:

$$\begin{aligned}\text{LHS} &= 2\text{E}\Re\left[e_a^*\varphi\right] \\ &= 2\text{E}\left[a_R\varphi_R - y_R\varphi_R + a_I\varphi_I - y_I\varphi_I\right] \\ &= 2\text{E}\left(a_R - y_R\right)_{\{|y_R|<R_R\}} - 2\text{E}\left(a_R - y_R\right)_{\{|y_R|>R_R\}} \\ &\quad + 2\text{E}\left(a_I - y_I\right)_{\{|y_I|<R_I\}} - 2\text{E}\left(a_I - y_I\right)_{\{|y_I|>R_I\}} \\ &= 2\text{E}\left(a_R - y_R\right) - 8\text{E}\left(a_R - y_R\right)_{\{y_R>R_R\}} \\ &\quad + 2\text{E}\left(a_I - y_I\right) - 8\text{E}\left(a_I - y_I\right)_{\{y_I>R_I\}}\end{aligned} \tag{42}$$

Exploiting assumption **A2**, we obtain

$$\begin{aligned}\text{LHS} &= 8\text{E}\left[\frac{1}{\sqrt{2\pi}}\exp\left(-\frac{(a_R - R_R)^2}{\zeta}\right)\sqrt{\frac{\zeta}{2}}\right] \\ &\quad + 8\text{E}\left[\frac{1}{\sqrt{2\pi}}\exp\left(-\frac{(a_I - R_I)^2}{\zeta}\right)\sqrt{\frac{\zeta}{2}}\right]\end{aligned} \tag{43}$$

Owing to four quadrant symmetry of QAM constellation, the moments evaluated for in-phase component are same as those for quadrature component. Simplifying and combining (41) and (43), we obtain

$$A - 2\mu\text{Tr}(\boldsymbol{R}) - \mu^{-1}\text{Tr}(\boldsymbol{Q}) = 0 \tag{44}$$

where $A := 16\text{E}\big[\frac{1}{\sqrt{2\pi}}\exp\big(-\frac{(a_R-R_R)^2}{\zeta}\big)\sqrt{\frac{\zeta}{2}}\big]$. Since the argument inside the exponent function, $(a_R - R_R)^2$, is always positive, we have $\exp(\cdot) = 0$ for $a_R \neq R_R$ and $\zeta \ll 1$. However, when $a_R = R_R$, we have $\exp(\cdot) = 1$ with probability $\text{P}_\text{r}[a_R = R_R]$. These considerations yield

$$A \approx \begin{cases} 0, & \text{if } a_R \neq R_R \\ \left(8\sqrt{\frac{\zeta}{\pi}}\right)\text{P}_\text{r}[a_R = R_R], & \text{if } a_R = R_R \end{cases} \tag{45}$$

Since an M-point constellation is being considered, the probability $\text{P}_\text{r}[a_R = R_R]$ is equal to $1/\sqrt{M}$. Rewriting the equality (44) as

$$8\sqrt{\frac{\zeta}{\pi M}} - 2\mu\text{Tr}(\boldsymbol{R}) - \mu^{-1}\text{Tr}(\boldsymbol{Q}) = 0 \tag{46}$$

Solving (46) for ζ, it follows directly that

$$\zeta_{\min}^{\text{MMA1-1}} = \left(\frac{\sqrt{\pi M}\left(2\mu\text{Tr}(\boldsymbol{R}) + \mu^{-1}\text{Tr}(\boldsymbol{Q})\right)}{8}\right)^2 \tag{47}$$

Denoting $c_1 := \frac{8}{\sqrt{\pi M}}$ and $c_2 := 2\text{Tr}(\boldsymbol{R})$, we obtain (T5.1). Further, substituting $\zeta = v^2$ and taking derivative with respect to μ, we obtain $c_1\frac{\text{d}v}{\text{d}\mu} - c_2 + \mu^{-2}\text{Tr}(\boldsymbol{Q}) = 0$. For the optimum value of μ, we have $\frac{\text{d}v}{\text{d}\mu} = 0$; solving this yields (T5.2). □

6. Comparison with existing methods

Some state of the art methods for EMSE analysis are available in literature, see [65,66,69]. In [66], Gouptil and Palicot developed a geometrical approach to steady-state analysis for Bussgang algorithms, and derived a closed-form analytical expression for EMSE, which when extended to tracking analysis is given as

$$\zeta \approx \frac{\mu\text{Tr}(\boldsymbol{R})\text{E}|\varphi|_{(a,a^*)}|^2 + \mu^{-1}\text{Tr}(\boldsymbol{Q})}{2\text{E}\frac{\partial^2}{\partial y\partial y^*}\Re[e_a^*\varphi]|_{(a,a^*)}} \tag{48}$$

It is important to note that this approach could be extended to certain algorithms which have continuous error-functions (like MMA2–2 and MMA1–2) in a straightforward manner to obtain approximate expressions which we have mentioned in Theorems 2 and 4. However, it becomes mathematically intractable to apply this approach for EMSE analysis of algorithms with discontinuous error-functions like MMA2–1 and MMA1–1, due to the fact that the required derivatives do not exit.

The EMSE expression by Gouptil and Palicot was based on circularity assumption for the *a priori* estimation error, e_a, i.e., $\text{E}e_a^2 = 0$. Without exploiting the circularity assumption, Lin et al. in [65] derived steady-state expressions utilizing Taylor series expansion. They obtained the following expressions:

$$\zeta \approx \frac{\mu\text{Tr}(\boldsymbol{R})\text{E}\left|\varphi|_{(a,a^*)}\right|^2 + \mu^{-1}\text{Tr}(\boldsymbol{Q})}{A_1 - \mu\text{Tr}(\boldsymbol{R})A_2}, \tag{49}$$

where

$$A_1 := -2\text{E}\Re\left(\frac{\partial\varphi}{\partial y}\bigg|_{(a,a^*)}\right) \tag{50}$$

and

$$A_2 := \text{E}\left|\frac{\partial\varphi}{\partial y}\bigg|_{(a,a^*)}\right|^2 + \text{E}\left|\frac{\partial\varphi}{\partial y^*}\bigg|_{(a,a^*)}\right|^2 + 2\text{E}\Re\left(\varphi^*\frac{\partial^2\varphi}{\partial y\partial y^*}\bigg|_{(a,a^*)}\right). \tag{51}$$

Table 1
EMSE in a non-stationary environment for four members of MMAp–q.

MMA2–2	$\frac{\mu \mathrm{Tr}(\boldsymbol{R}) d_1 + \mu^{-1}\mathrm{Tr}(\boldsymbol{Q})}{d_2 - \mu \mathrm{Tr}(\boldsymbol{R}) d_3}$, where $d_1 = \mathrm{E}a_R^6 - 2R_R^2 \mathrm{E}a_R^4 + R_R^4 \mathrm{E}a_R^2$, $d_2 = 6\mathrm{E}a_R^2 - 2R_R^2$, $d_3 = 3\mathrm{E}a_R^4 + R_R^4$
MMA2–1	$\left(\frac{-d_1 + \sqrt{d_1^2 + d_2(\mu \mathrm{Tr}(\boldsymbol{R}) + \mu^{-1}\mathrm{Tr}(\boldsymbol{Q})) - 2\mathrm{Tr}(\boldsymbol{Q})(\mu \mathrm{Tr}(\boldsymbol{R}) + \mathrm{Tr}(\boldsymbol{Q}))}}{d_2 + 4 - \mu \mathrm{Tr}(\boldsymbol{R})} \right)^2$ where $d_1 = \frac{8R_R}{\sqrt{\pi M}}$, $d_2 = 8\left(\frac{2}{\sqrt{M}} - 1\right)$
MMA1–2	$\frac{2\mu \mathrm{Tr}(\boldsymbol{R}) \mathrm{E}(R_R - \lvert a_R \rvert)^2 + \mu^{-1}\mathrm{Tr}(\boldsymbol{Q})}{2 - \mu \mathrm{Tr}(\boldsymbol{R})}$
MMA1–1	$\frac{\pi M \left(2\mu \mathrm{Tr}(\boldsymbol{R}) + \mu^{-1}\mathrm{Tr}(\boldsymbol{Q})\right)^2}{64}$

Table 2
Optimum step-size in a non-stationary environment for four members of MMAp–q.

MMA2–2	$\frac{\sqrt{\mathrm{Tr}(\boldsymbol{Q})\mathrm{Tr}(\boldsymbol{R}) d_1 d_2^2 + \mathrm{Tr}(\boldsymbol{Q})^2 \mathrm{Tr}(\boldsymbol{R})^2 d_3^2} - \mathrm{Tr}(\boldsymbol{Q})\mathrm{Tr}(\boldsymbol{R}) d_3}{\mathrm{Tr}(\boldsymbol{R}) d_1 d_2}$, where $d_1 = \mathrm{E}a_R^6 - 2R_R^2 \mathrm{E}a_R^4 + R_R^4 \mathrm{E}a_R^2$, $d_2 = 6\mathrm{E}a_R^2 - 2R_R^2$, $d_3 = 3\mathrm{E}a_R^4 + R_R^4$
MMA2–1	$\sqrt{\frac{\mathrm{Tr}(\boldsymbol{Q})}{\mathrm{Tr}(\boldsymbol{R}) P_a}}$
MMA1–2	$\sqrt{\frac{\mathrm{Tr}(\boldsymbol{Q})}{2\mathrm{Tr}(\boldsymbol{R}) \mathrm{E}(R_R - \lvert a_R \rvert)^2}}$
MMA1–1	$\sqrt{\frac{\mathrm{Tr}(\boldsymbol{Q})}{2\mathrm{Tr}(\boldsymbol{R})}}$

Similar to (48), the expressions (49)–(51) involve the evaluation of derivatives. In case of continuous error-functions, the EMSE analysis can be carried out by this approach, but is not applicable to the case of discontinuous error-functions. It is important to note that we have originally provided the accurate and closed-form (under certain assumptions) expressions for steady-state EMSE for different multimodulus equalizers. However, the approaches proposed by Gouptil and Palicot and Lin et al., only applicable for algorithms with continuous error-function, and therefore cannot be extended to algorithms with discontinuous error-functions.

In [69], Naffouri and Sayed proposed an ingenious approach for the evaluation of EMSE by exploiting fundamental energy conservation relation and Price theorem. The proposed EMSE expression is given as

$$\zeta = \frac{\mu \mathrm{Tr}(\boldsymbol{R}) h_U(\zeta) + \mu^{-1}\mathrm{Tr}(\boldsymbol{Q})}{2h_G(\zeta)}, \tag{52}$$

where

$$h_U(\zeta) \triangleq \mathrm{E}|\varphi|^2 \tag{53}$$

and

$$h_G(\zeta) \triangleq \frac{\mathrm{E}\Re[e_a^* \varphi]}{\mathrm{E}|e_a|^2}. \tag{54}$$

The result (52)–(54) corroborate the expressions that we have obtained for different multimodulus equalizers.

7. Simulation results

In this section, we verify the tracking performance analyses for MMA2–2, MMA2–1, MMA1–2 and MMA1–1 (as summarized in Tables 1 and 2). The experiments have been performed considering (i) comparison with state of the art methods, (ii) a time-varying channel (with a constant mean part and an autoregressive random part), (iii) the effect of filter-length on equalization performance, and (iv) equalizing an optical channel for adaptive polarization demultiplexing.

7.1. Experiment I: Considering zero-forcing solution

In this experiment, the elements of perturbation vector $\boldsymbol{q}_n$ are modeled as zero mean wide-sense stationary and mutually uncorrelated. The corresponding positive definite autocorrelation matrix of $\boldsymbol{q}_n$ is obtained as $\boldsymbol{Q} = \sigma_q^2 \boldsymbol{I}$ (where $\sigma_q = 10^{-3}$).[3] The simulated EMSE have been obtained for equalizer lengths $N = 7$ and $N = 11$ for 16-QAM signals. The values of $R_R = R_I$ are equal to 8.2, 3, 2.5 and 31 for MMA2–2, MMA2–1, MMA1–2 and MMA1–1 for 16-QAM signals, respectively. Each simulated trace is obtained by performing 100 independent runs where each run is executed for 5×10^3 iterations. Note that, due to assuming an already equalized scenario, we do not have to worry about the iterations required for successful convergence of the equalizer; thus the EMSE is computed for all iterations. The Monte-Carlo simulation requires to add the perturbation $\boldsymbol{q}_n$ directly in the weight update process. The weight update, in this experiment, is thus governed by

$$\boldsymbol{w}_n^o = \boldsymbol{w}_{n-1}^o + \mu \varphi(y_n)^* \boldsymbol{x}_n + \boldsymbol{q}_n \tag{55}$$

The terms containing the step-size μ and $\boldsymbol{q}_n$ contribute to tracking and acquisition errors [14]. The rule (55) has been adopted in [14, 48–50,61].

Since the steady-state EMSE of the MMA algorithms is composed of two (tracking and acquisition) errors. The tracking error decreases with μ and increases with the system non-stationarity variance $\mathrm{Tr}(\boldsymbol{Q})$. The acquisition error increases with μ and the received signal variance $\mathrm{Tr}(\boldsymbol{R})$, thus, the resulting EMSE is a convex downward (bowl shaped) function of step-size μ. Noticeably, for all simulation cases, the analytically obtained minimum EMSE ($\zeta_{\min}^{\mathrm{MMA}p-q}$) and the optimum step-size ($\mu_{\mathrm{opt}}^{\mathrm{MMA}p-q}$), are marked, respectively, with markers $\triangleright$ and $\Diamond$. Refer to Figs. 3(a) and 4(a) for the comparison of analytical and simulated EMSE of MMA2–2 equalizer. The legends 'Numerical' and 'Closed-from' refer to the solutions (21) and (T2.1), respectively. It is evident from this result that, for 16-QAM with smaller filter length (i.e., $N = 7$), the numerical, the closed-form and the simulated traces conform each other for all values of step-sizes. However, for larger filter length (i.e., $N = 11$), traces start deviating from each other for higher values of EMSE.

Next, refer to Figs. 3(b) and 4(b) in which the analytical and simulated EMSE of MMA2–1 equalizer are compared. The legends 'Numerical' and 'Closed-from' refer to the solutions (28) and (T3.1), respectively. It can be observed from the results that, for 16-QAM, the numerical, the closed-form and the simulated traces conform each other for all values of step-sizes for both filter length ($N = 7$ and $N = 11$). Figs. 3(c) and 4(c) compare the analytical and simulated EMSE of MMA1–2 equalizer. The legends 'Numerical' and 'Closed-from' refer to the solutions (36) and (T4.1), respectively. It is evident from the results that both expressions (numerical and closed-form) are in good agreement with the simulated traces for 16-QAM for both filter length ($N = 7$ and $N = 11$). Similarly, refer to Figs. 3(d) and 4(d) which compare the analytical and simulated EMSE of MMA1–1 equalizer. The legends 'Numerical' and 'Closed-from' refer to the solutions (44) and (T5.1), respectively. It is evident from this result that, for 16-QAM for both filter length ($N = 7$ and $N = 11$), the numerical, the closed-form and the simulated traces conform each other for all values of step-sizes.

Here we observe that the numerical results deviate from Monte-Carlo results when the step-size is far away from the opti-

[3] Note that this modeling (i.e., zero off-diagonal elements in $\boldsymbol{Q}$) is justified in the light of our analytical findings in Theorems 2, 3, 4 and 5 which imply that the EMSE depends neither on the individual diagonal elements nor the off-diagonal elements of matrix $\boldsymbol{Q}$, but rather depends on $\mathrm{Tr}(\boldsymbol{Q})$. In other words, given the sum of the mean square fluctuations of the elements of $\boldsymbol{q}_n$, the EMSE does not depend on the contribution of individual elements.

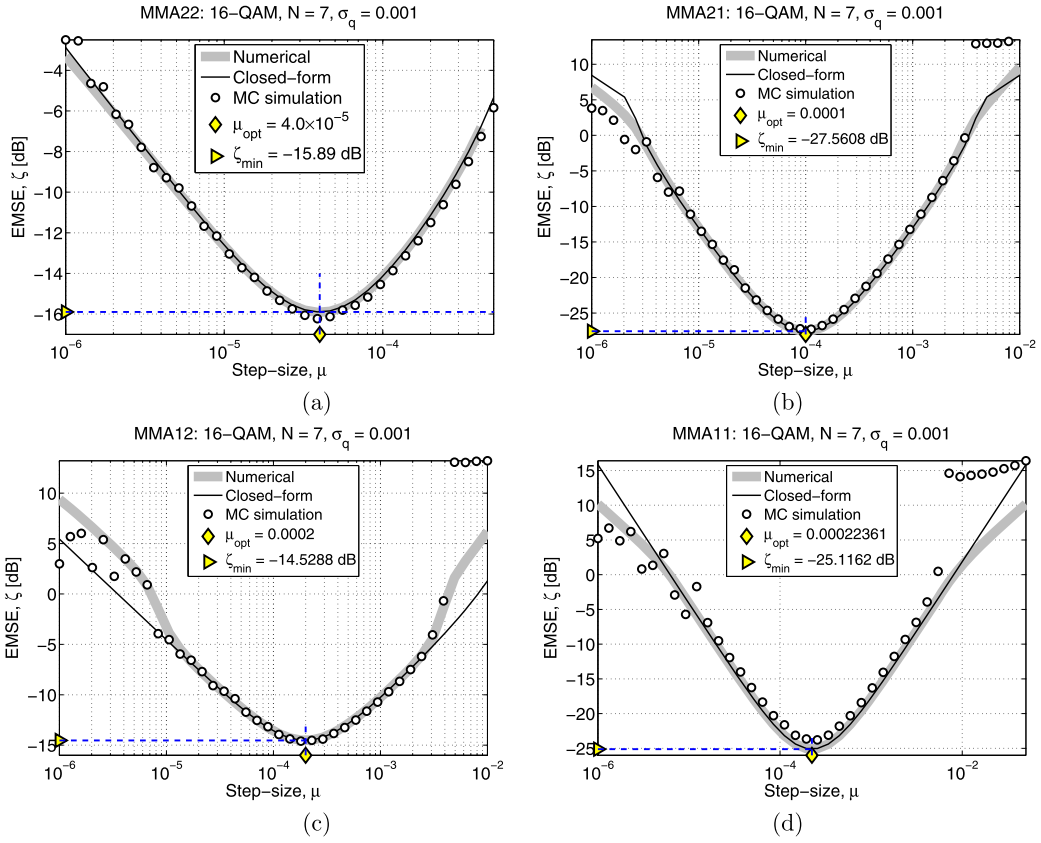

Fig. 3. EMSE traces for $N = 7$ and 16-QAM.

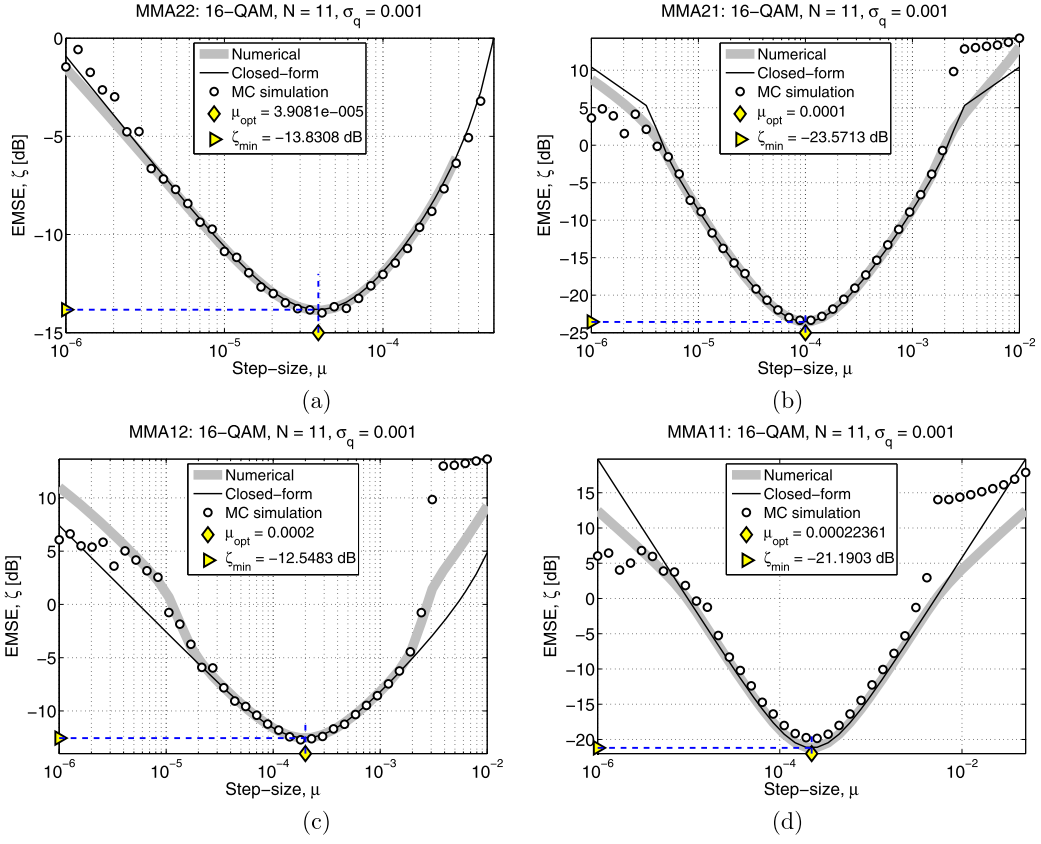

Fig. 4. EMSE traces for $N = 11$ and 16-QAM.

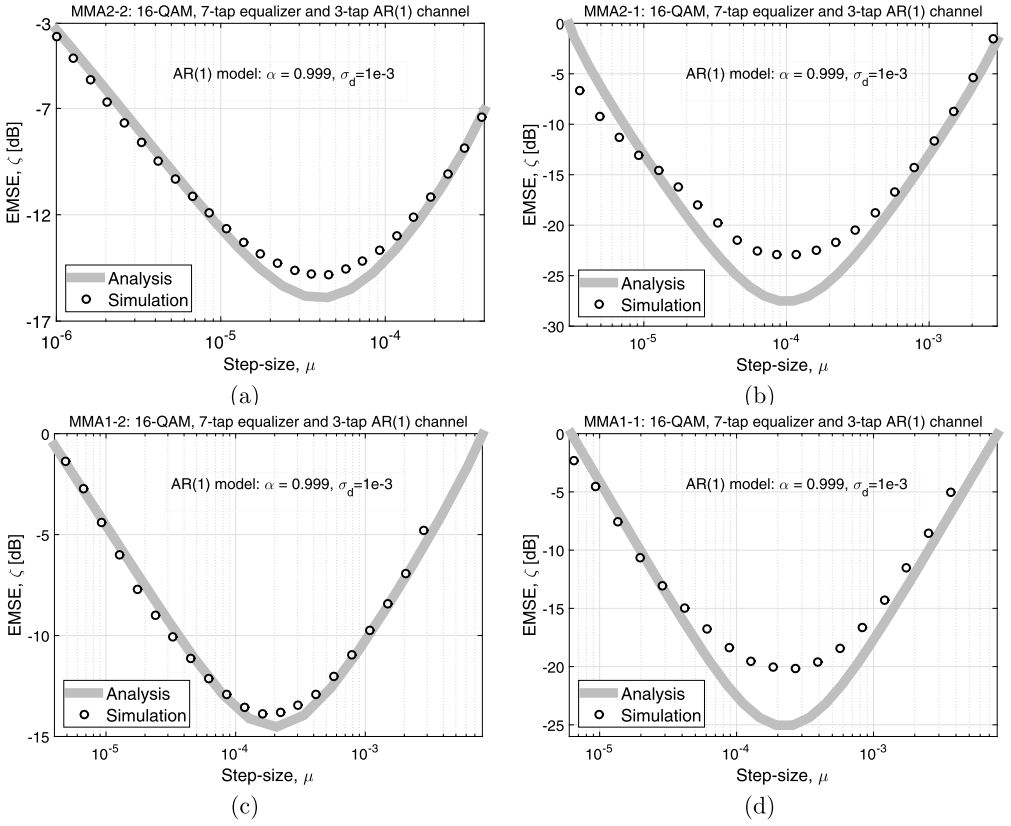

Fig. 5. EMSE traces for four members of MMAp–q with 16-QAM signaling on `channel-1`. For $f_D T = 0.01$ and unit lag, we have $\alpha = 0.999$.

mum step-size. We emphasize at the fact that the EMSE expressions obtained (in this work) are valid only for sufficiently small step-sizes. It is also important to note that there are upper bounds on the step-sizes above which an adaptive filter cannot provide any useful output. The reason why EMSE analytical trace deviates from the simulated ones at very small step-size is not completely understood at this stage.

7.2. Experiment II: Equalizing time-varying channel

We evaluate the performance analysis of the addressed equalizers in the presence of a time-varying (TV) channel. A TV channel is usually modeled such that its autocorrelation properties correspond to wide-sense stationary and uncorrelated scattering (WSSUS) (as suggested by Bello [71]). However, as reported in [72], a first-order (Gauss–Markov) autoregressive model is sufficient enough to model a slow-varying channel, where the channel at index n is given as $\boldsymbol{h}_n = \boldsymbol{h}_{\text{const}} + \boldsymbol{c}_n$. The channel is a complex Gaussian random process with a constant mean $\boldsymbol{h}_{\text{const}}$ (because of shadowing, reflections, and large scale path loss) and a time-variant part $\boldsymbol{c}_n$, which is a first-order Markov process as given by $\boldsymbol{c}_n = \alpha \boldsymbol{c}_{n-1} + \boldsymbol{d}_n$ where α is a constant, and the vector $\boldsymbol{d}_n$ is a zero-mean i.i.d. circular complex Gaussian process with correlation matrix $\boldsymbol{D}$.[4] The channel taps varies from symbol to symbol and are modeled as mutually uncorrelated circular complex Gaussian random processes. The time-varying part of the channel can be modeled by a pth-order autoregressive process AR(p). The matrix $\boldsymbol{D}$, due to WSSUS assumption, is diagonal and each of its diagonal element is σ_d^2. In the present scenario, we consider $\sigma_d^2 = 1\times10^{-3}$, $\alpha = 0.999$, and $\boldsymbol{h}_{\text{const}} = [1+0.2j, -0.2+0.1j, 0.1-0.1j]^T$ using a 7-tap baud-spaced equalizer with 16-QAM signaling. Refer to Fig. 5 for the comparison of theoretical and simulated EMSE of MMA2–2, MMA2–1, MMA1–2 and MMA1–1 equalizers. The legend 'Analysis' refers to the solutions (T2.1), (T3.1), (T4.1) and (T5.1) for MMA2–2, MMA2–1, MMA1–2 and MMA1–1 equalizers, respectively. It is evident from the results that the theoretical and simulated EMSE traces conform each other. Note that the factor $\text{Tr}(\boldsymbol{Q})$ has been replaced with $\text{Tr}(\boldsymbol{D})$ in the evaluation of analytical EMSE. In the sequel, we refer to this channel as `channel-1`.

7.3. Experiment III: Effect of filter-length on EMSE

In the previous experiment, we considered a TV channel where the effect of filter-length on equalization capability has not been taken into consideration. It is widely known that a reasonable filter-length is required to equalize successfully a propagation channel. An insufficient filter-length introduces an additional distortion which we have not considered in Theorems 2, 3, 4, and 5. However, as mentioned in [3], the distortive effect of insufficient filter-length may easily be incorporated (in the EMSE expressions) as an additive term; the total EMSE, which we denote as TEMSE, is thus given as follows:

$$\text{TEMSE} = \underbrace{\lim_{n\to\infty} \text{E}|e_{a,n}|^2}_{=:\zeta} + \underbrace{\text{E}|a_n|^2 \|\mathcal{H}\boldsymbol{w}^{o*} - \boldsymbol{e}\|^2}_{=:\chi} \tag{56}$$

where ζ is EMSE as we obtained in Theorems 2, 3, 4 and 5, and χ is the additional squared error contributed by the (insufficient)

[4] For an AR(1) system, $\alpha = \mathcal{J}_o(2\pi f_D T)$, which makes the autocorrelation of the taps modeled by $\boldsymbol{c}_n = \alpha \boldsymbol{c}_{n-1} + \boldsymbol{d}_n$ equal the true autocorrelation at unit lag (where $\mathcal{J}_o$ is the zero-order Bessel function of the first kind, f_D is the Doppler rate and T is the baud duration). The parameter α determines the rate of the channel variation while the variances $\sigma_{d,i}^2$ of the ith entry of $\boldsymbol{d}_n$ determines the magnitude of the variation. So, α and $\sigma_{d,i}^2$ determines how "fast" and how "much" the time-varying part $c_{n,i}$ of each channel tap $h_{n,i}$ varies with respect to the known mean of that tap $h_{\text{const},i}$. The value of α can be estimated from the estimate of f_D. Similarly, given the average energy of the ith part of $\boldsymbol{c}_n$, $\text{E}|c_{n,i}|^2$, the value of $\sigma_{d,i}$ is evaluated as [72] $\sigma_{d,i} = |h_{\text{const},i}|^2\sqrt{1-\alpha^2}\big/\sqrt{\text{E}|c_{n,i}|^2}$.

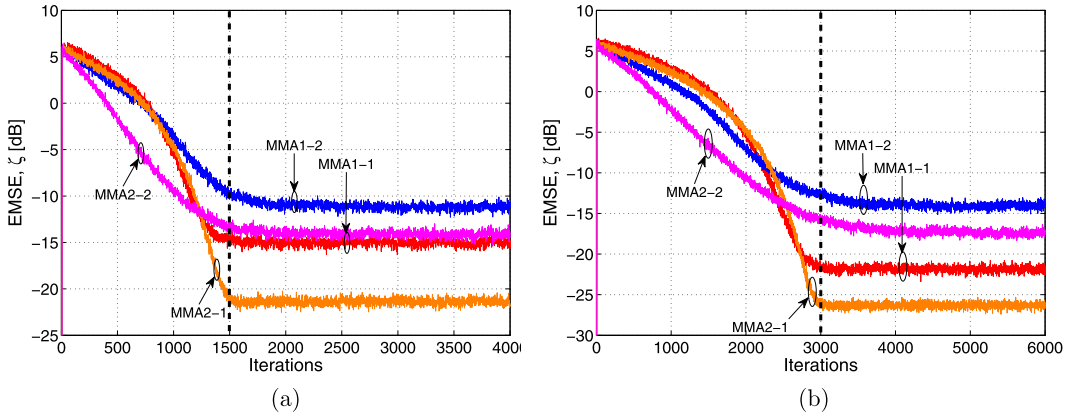

Fig. 6. Transient EMSE traces for MMAp–q with 16-QAM signaling on `channel-2`.

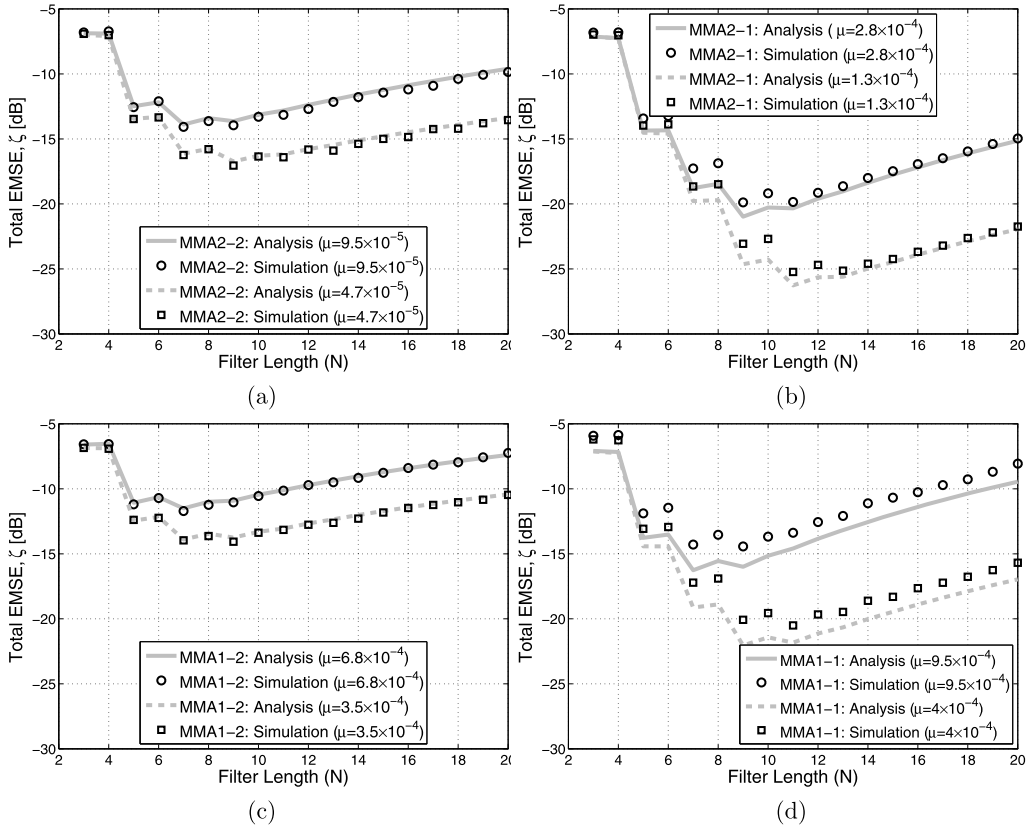

Fig. 7. EMSE traces considering the effect of filter-length on `channel-2`. (a) The optimal filter-length for MMA2–2 is found to be 7 and 9 for 9.5×10^{-5} and 4.7×10^{-5} respectively, (b) The optimal filter-length for MMA2–1 is found to be 9 and 11 for 2.8×10^{-3} and 1.3×10^{-4}, (c) The optimal filter-length for MMA1–2 is found to be 7 for both 6.8×10^{-4} and 3.5×10^{-4}, (d) The optimal filter-length for MMA1–1 is found to be 7 and 9 for 9.5×10^{-4} and 4×10^{-4} respectively.

filter-length. The vector $\boldsymbol{w}^o$ is zero-forcing solution, $\mathcal{H}$ is channel matrix, and $\boldsymbol{e}$ is overall idealistic (single-spike) channel-equalizer impulse response as defined in Section 2.

Note that the EMSE, ζ, is proportional to filter-length for the given step-size. The parameter χ on the other hand decreases with filter-length.[5] In our simulation, the value of optimal weight vector, $\boldsymbol{w}^o$, is obtained as $\boldsymbol{w}^o = \texttt{pinv}(\mathcal{H})\boldsymbol{e}$ where $\texttt{pinv}(\cdot)$ is the MATLAB function for the evaluation of pseudo-inverse. The TEMSE, as expressed in (56), is a convex downward function of filter-length. Evaluating TEMSE for different filter lengths can provide us with the optimal value of filter-length required to equalize the given channel and given step-size. In this simulation, we have considered a voice-band telephone channel $\boldsymbol{h}_n = [-0.005 - 0.004j, 0.009 + 0.03j, -0.024 - 0.104j, 0.854 + 0.52j, -0.218 + 0.273j, 0.049 - 0.074j, -0.016 + 0.02j]$ [73] and 16-QAM signaling. The eigenvalue spread of the channel is 5.83 and the ISI introduced by this channel is -8.44 dB. In the sequel, we refer to this channel as `channel-2`.

The two different values of step-size (μ) are chosen such that the equalizers converge to steady-state around 1500 iterations and 3000 iterations, as depicted in Fig. 6. All simulation points were

[5] The actual expression of χ (as denoted by D_f in [3, Eq. 4.8.24]) contains an equalizer solution (as denoted by $\overline{\boldsymbol{\theta}}$) that also depends on blind equalization error-function. However, we have observed that the true value of $\overline{\boldsymbol{\theta}}$ is very close to $\mathcal{H}^+\boldsymbol{e}$ for all four addressed members of MMAp–q where $(\cdot)^+$ denotes pseudo-inverse. So, in this work, we have replaced the true expression of $\overline{\boldsymbol{\theta}}$ with its simplified form $\boldsymbol{w}^{o*} = \mathcal{H}^+\boldsymbol{e}$ and our simulation findings (as depicted in Fig. 7) validate that this simplification is reasonable.

obtained by executing the program 10 times (or runs) with random and independent generation of transmitted data. Each run was executed for as many iterations as required for the convergence. Once convergence is acquired, the equalizer is run for further 5000 iterations for the computation of steady-state value of EMSE. In Fig. 7, we depict analytical and simulated TEMSE obtained as a function of filter-length for the given step-sizes for MMA2–2, MMA2–1, MMA1–2 and MMA1–1. Both analytical and simulated TEMSE are found to be in close agreement.

7.4. Experiment IV: Adaptive polarization demultiplexing

In this experiment we consider an adaptive optical demultiplexing scenario. A key part of the digital signal processing receiver unit is to demultiplex the received signal to recover the two orthogonal polarization tributaries sent from the transmitter end. This can be done using blind adaptive FIR filters, updated using the stochastic gradient algorithm (employing only the demultiplexed sequence) as proposed in [28]. The filters are arranged in a butterfly structure [74] as shown in Fig. 8 and are continuously updated. Note that the multiplexing phenomenon can be modeled as a *Jones matrix*. Given the azimuth rotation angle 2θ and the elevation rotation angle ϕ, the unitary 2×2 (Jones) matrix $\boldsymbol{\mathcal{R}}$, which represents the baseband model of two multiplexed optical channels, is given by [29]

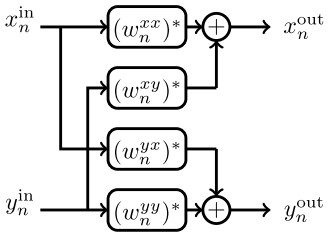

Fig. 8. Optical butterfly equalizer.

$$\boldsymbol{\mathcal{R}}(\theta,\phi)=\begin{bmatrix}\cos(\theta) & \sin(\theta)\exp(-j\phi)\\ -\exp(j\phi)\sin(\theta) & \cos(\theta)\end{bmatrix}. \tag{57}$$

Note that the two rows represent multiplexed channels which rotate the horizontal and vertical states of polarized transmitted data and convert them into a new but arbitrary pair of orthogonal states. Suppose x_n and y_n are the transmitted polarization division multiplexed QAM (PDM-QAM) signals, using the channel model, the received polarized signals (which become input to the demultiplexer) are

$$\begin{bmatrix}x_n^{\text{in}}\\ y_n^{\text{in}}\end{bmatrix}=\boldsymbol{\mathcal{R}}\begin{bmatrix}x_n\\ y_n\end{bmatrix} \tag{58}$$

It has to be noted that the two input signals of the block, x_n^{in} and y_n^{in}, are a mixture of the two signals emitted along the two orthogonal states of polarization of light. Therefore the task of the adaptive equalizer is to estimate the inverse of the Jones matrix so as to reverse the effects induced by the channel propagation. The adaptive equalizer (demultiplexer) $\boldsymbol{w}_n$ is an adaptive 2×2 matrix and is defined as $\boldsymbol{w}_n=\begin{bmatrix}w_n^{xx} & w_n^{xy};\ & w_n^{yx} & w_n^{yy}\end{bmatrix}$. The demultiplexed signals, x_n^{out} and y_n^{out}, are given by

$$\begin{bmatrix}x_n^{\text{out}}\\ y_n^{\text{out}}\end{bmatrix}=\boldsymbol{w}_n^*\begin{bmatrix}x_n^{\text{in}}\\ y_n^{\text{in}}\end{bmatrix}=\begin{bmatrix}(w_n^{xx})^*x_n^{\text{in}}+(w_n^{xy})^*y_n^{\text{in}}\\ (w_n^{yx})^*x_n^{\text{in}}+(w_n^{yy})^*y_n^{\text{in}}\end{bmatrix} \tag{59}$$

Upon successful convergence of $\boldsymbol{w}_n$, x_n^{out} and y_n^{out} are required to provide estimates of x_n and y_n, respectively. Due to permutation ambiguity (also known as channel swapping), however, it is possible that x_n^{out} and y_n^{out}, instead, provide estimates of y_n and x_n, respectively.[6]

Since the Jones matrix is considered to be stationary, we have $\sigma_q=0$ for the analytical evaluation of EMSE. Refer to Fig. 9(a) for

[6] For some values of θ and ϕ, we have found that some members of MMAp–q happen to recover the signals with poor output signal-to-noise ratio. However, discussing those cases and their remedies are beyond the scope of this work and will be discussed else where.

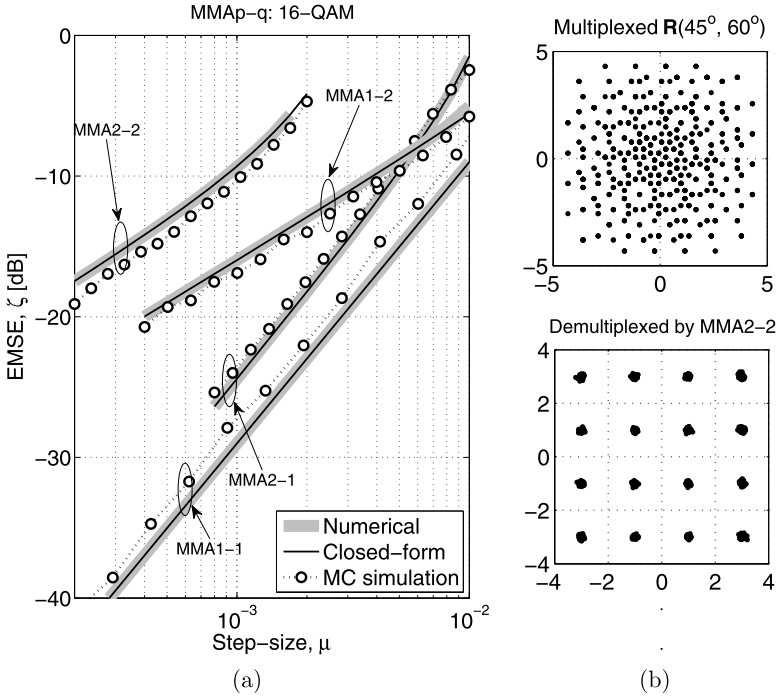

Fig. 9. (a) EMSE traces for four members of MMAp–q with 16-QAM signaling for $\boldsymbol{\mathcal{R}}(45^\circ, 60^\circ)$. (b) Scatter plots before and after demultiplexing using MMA2–2 equalizer with $\mu=1\times 10^{-4}$ (subplots for other equalizers are not shown due to space limitation).

the comparison of theoretical and simulated EMSE of MMA2–2, MMA2–1, MMA1–2 and MMA1–1 equalizers for $\mathcal{R}(45°, 60°)$. The legend 'Closed-form' refers to the solutions (T2.1), (T3.1), (T4.1) and (T5.1) and the legend 'Numerical' refers to (21), (28), (36) and (44) for MMA2–2, MMA2–1, MMA1–2 and MMA1–1 equalizers, respectively. As evident from (59), we use $N = 2$ for the evaluation of analytical EMSE. Also refer to Fig. 9(b) for the scatter plots for received (multiplexed) and equalized (demultiplexed) signals.

8. Conclusions

This paper reports the steady-state EMSE analysis of adaptive filters belonging to MMAp–q family (i.e., MMA2–2, MMA2–1, MMA1–2 and MMA1–1) by exploiting the fundamental energy relation in non-stationary environment. This relation is fundamental in that it is exact, and it holds without requiring any approximation. Exploiting this relation, we have obtained analytical (closed-form) expressions for EMSE for MMA2–2, MMA2–1, MMA1–2 and MMA1–1 equalizers are verified by computer simulations. From this study, we conclude the following:

1. By using fundamental variance relation, steady-state EMSE analysis for different MMAp–q equalizers can be performed in a simpler way. In particular, we have obtained exact as well as approximate (but closed-form) EMSE expressions for MMA2–2, MMA2–1, MMA1–2 and MMA1–1 equalizers using the fundamental variance relation in a straightforward manner. Our analytical findings have been validated for both stationary and non-stationary channel environments. Among the four addressed members of MMAp–q, we have also noticed that MMA2–1 is providing the least EMSE in multi-path channel environment.
2. The so-called total EMSE expression has been found useful in determining the optimum lengths of the addressed equalizers for underlying channels and given values of step-sizes. Our experiments have indicated that the optimum lengths for MMA2–2, MMA2–1, MMA1–2 and MMA1–1 equalizers for a typical (7-tap) voice-band channel are between 7 and 13 dependent upon the step-size.
3. There has been a growing trend of application of different variants of MMA and CMA in optical systems for polarization demultiplexing supported with coherent detection. We have evaluated the performance of MMAp–q algorithms in terms of EMSE for the task of adaptive polarization demultiplexing in coherent optical systems.

Acknowledgments

The authors acknowledge the support of COMSATS Institute of Information Technology (Islamabad and Wah Campuses), Pakistan, the Deanship of Scientific Research at King Fahd University of Petroleum and Minerals under research grant RG1414, Saudi Arabia, and Brunel University London, UK towards the accomplishment of this work. They also acknowledge the Editor and anonymous reviewers for their support and valuable feedback.

Appendix A. Supplementary material

Supplementary material related to this article can be found online at http://dx.doi.org/10.1016/j.dsp.2015.09.002.

References

[1] S. Haykin, Blind Deconvolution, PTR Prentice Hall, Englewood Cliffs, 1994.
[2] R. Johnson Jr., P. Schniter, T.J. Endres, J.D. Behm, D.R. Brown, R.A. Casas, Blind equalization using the constant modulus criterion: a review, Proc. IEEE 86 (10) (1998) 1927–1950.
[3] Z. Ding, Y. Li, Blind Equalization and Identification, Marcel Dekker, Inc., New York, Basel, 2001.
[4] B. Friedlander, Lattice filters for adaptive processing, IEEE Proc. 70 (8) (1982) 829–867.
[5] S.J. Orfanidis, Optimum Signal Processing: An Introduction, Macmillan, New York, 1985.
[6] B. Widrow, J.R. Glover Jr., J.M. McCool, J. Kaunitz, C.S. Williams, R.H. Hearn, J.R. Zeidler, E. Dong Jr., R.C. Goodlin, Adaptive noise cancelling: principles and applications, IEEE Proc. 63 (12) (1975) 1692–1716.
[7] S.L. Marple Jr., Digital Spectral Analysis with Applications, vol. 1, Prentice-Hall, Inc., Englewood Cliffs, NJ, 1987.
[8] B. Widrow, S.D. Stearns, Adaptive Signal Processing, vol. 1, Prentice-Hall, Inc., Englewood Cliffs, NJ, 1985.
[9] C.F.N. Cowan, P.M. Grant, P.F. Adams, Adaptive Filters, vol. 152, Prentice-Hall, Englewood Cliffs, 1985.
[10] S. Haykin, Introduction to Adaptive Filters, vol. 984, Macmillan, New York, 1984.
[11] M.L. Honig, D.G. Messerschmitt, Adaptive Filters: Structures, Algorithms, and Applications, Kluwer, 1984.
[12] S.T. Alexander, Adaptive Signal Processing: Theory and Applications, Springer-Verlag, New York, 1986.
[13] B. Widrow, J.M. McCool, M. Larimore, C.R. Johnson Jr., Stationary and nonstationary learning characteristics of the LMS adaptive filter, IEEE Proc. 64 (8) (1976) 1151–1162.
[14] A.H. Sayed, Fundamentals of Adaptive Filtering, John Wiley & Sons, Hoboken, New Jersey, 2003.
[15] D. Godard, Self-recovering equalization and carrier tracking in two-dimensional data communication systems, IEEE Trans. Commun. 28 (11) (1980) 1867–1875.
[16] J. Treichler, M. Larimore, New processing techniques based on the constant modulus adaptive algorithm, IEEE Trans. Acoust. Speech Signal Process. 33 (2) (1985) 420–431.
[17] S. Abrar, A. Zerguine, A.K. Nandi, Adaptive blind channel equalization, in: C. Palanisamy (Ed.), Digital Communication, InTech Publishers, Rijeka, Croatia, 2012, Chapter 6.
[18] A. Benveniste, M. Goursat, Blind equalizers, IEEE Trans. Commun. 32 (8) (1984) 871–883.
[19] K. Wesolowski, Self-recovering adaptive equalization algorithms for digital radio and voiceband data modems, in: Proc. European Conf. Circuit Theory and Design, 1987, pp. 19–24.
[20] K.N. Oh, Y.O. Chin, Modified constant modulus algorithm: blind equalization and carrier phase recovery algorithm, in: Proc. IEEE Globcom, 1995, pp. 498–502.
[21] G.-H. Im, C.-J. Park, H.-C. Won, A blind equalization with the sign algorithm for broadband access, IEEE Commun. Lett. 5 (2) (2001) 70–72.
[22] S. Abrar, A.K. Nandi, Blind equalization of square-QAM signals: a multimodulus approach, IEEE Trans. Commun. 58 (6) (2010) 1674–1685.
[23] K. Wesolowski, Analysis and properties of the modified constant modulus algorithm for blind equalization, Eur. Trans. Telecommun. 3 (3) (1992) 225–230.
[24] J. Yang, J.-J. Werner, G.A. Dumont, The multimodulus blind equalization and its generalized algorithms, IEEE J. Sel. Areas Commun. 20 (5) (2002) 997–1015.
[25] J.-T. Yuan, K.-D. Tsai, Analysis of the multimodulus blind equalization algorithm in QAM communication systems, IEEE Trans. Commun. 53 (9) (2005) 1427–1431.
[26] X.-L. Li, W.-J. Zeng, Performance analysis and adaptive Newton algorithms of multimodulus blind equalization criterion, Signal Process. 89 (11) (2009) 2263–2273.
[27] J.-T. Yuan, T.-C. Lin, Equalization and carrier phase recovery of CMA and MMA in blind adaptive receivers, IEEE Trans. Signal Process. 58 (6) (2010) 3206–3217.
[28] K. Kikuchi, Polarization-demultiplexing algorithm in the digital coherent receiver, in: Proc. Digest 2008 IEEE/LEOS Summer Topical Meetings, 2008, pp. 101–102.
[29] S.J. Savory, Digital coherent optical receivers: algorithms and subsystems, IEEE J. Sel. Top. Quantum Electron. 16 (5) (2010) 1164–1179.
[30] E.M. Ip, J.M. Kahn, Fiber impairment compensation using coherent detection and digital signal processing, J. Lightwave Technol. 28 (4) (2010) 502–519.
[31] J. Renaudier, O. Bertran-Pardo, G. Charlet, M. Salsi, H. Mardoyan, P. Tran, S. Bigo, 8 Tb/s long haul transmission over low dispersion fibers using 100 Gb/s PDM-QPSK channels paired with coherent detection, Bell Labs Tech. J. 14 (4) (2010) 27–45.
[32] P. Johannisson, M. Sjödin, M. Karlsson, H. Wymeersch, E. Agrell, P.A. Andrekson, Modified constant modulus algorithm for polarization-switched QPSK, Opt. Express 19 (8) (2011) 7734–7741.
[33] D.S. Millar, S.J. Savory, Blind adaptive equalization of polarization-switched QPSK modulation, Opt. Express 19 (9) (2011) 8533–8538.
[34] I. Roudas, A. Vgenis, C.S. Petrou, D. Toumpakaris, J. Hurley, M. Sauer, J. Downie, Y. Mauro, S. Raghavan, Optimal polarization demultiplexing for coherent optical communications systems, J. Lightwave Technol. 28 (7) (2010) 1121–1134.
[35] A. Vgenis, C.S. Petrou, C.B. Papadias, I. Roudas, L. Raptis, Nonsingular constant modulus equalizer for PDM-QPSK coherent optical receivers, IEEE Photonics Technol. Lett. 22 (1) (2010) 45–47.

[36] I. Fatadin, D. Ives, S.J. Savory, Blind equalization and carrier phase recovery in a 16-QAM optical coherent system, J. Lightwave Technol. 27 (15) (2009) 3042–3049.
[37] P. Johannisson, H. Wymeersch, M. Sjödin, A.S. Tan, E. Agrell, P.A. Andrekson, M. Karlsson, Convergence comparison of the CMA and ICA for blind polarization demultiplexing, J. Opt. Commun. Netw. 3 (6) (2011) 493–501.
[38] C. Yuxin, H. Guijun, Y. Li, Z. Ling, L. Li, Mode demultiplexing based on multi-modulus blind equalization algorithm, Opt. Commun. 324 (2014) 311–317.
[39] Z. Qu, S. Fu, M. Zhang, M. Tang, P. Shum, D. Liu, Analytical investigation on self-homodyne coherent system based on few-mode fiber, IEEE Photonics Technol. Lett. 26 (1) (2014) 74–77.
[40] J. Zhang, B. Huang, X. Li, Improved quadrature duobinary system performance using multi-modulus equalization, IEEE Photonics Technol. Lett. 25 (16) (2013) 1630–1633.
[41] J. Zhang, J. Yu, N. Chi, Z. Dong, J. Yu, X. Li, L. Tao, Y. Shao, Multi-modulus blind equalizations for coherent quadrature duobinary spectrum shaped pm-qpsk digital signal processing, J. Lightwave Technol. 31 (7) (2013) 1073–1078.
[42] Z. Yu, X. Yi, J. Zhang, M. Deng, H. Zhang, K. Qiu, Modified constant modulus algorithm with polarization demultiplexing in Stokes space in optical coherent receiver, J. Lightwave Technol. 31 (19) (2013) 3203–3209.
[43] X. Zhou, J. Yu, M.F. Huang, Y. Shao, T. Wang, P. Magill, M. Cvijetic, L. Nelson, M. Birk, G. Zhang, S. Ten, H.B. Matthew, S.K. Mishra, Transmission of 32-Tb/s capacity over 580 km using RZ-shaped PDM-8QAM modulation format and cascaded multimodulus blind equalization algorithm, J. Lightwave Technol. 28 (4) (2010) 456–465.
[44] S. Abrar, A.K. Nandi, Adaptive solution for blind equalization and carrier-phase recovery of square-QAM, IEEE Signal Process. Lett. 17 (9) (2010) 791–794.
[45] S. Abrar, A. Zerguine, A.K. Nandi, Blind adaptive polarization demultiplexing in coherent PDM QAM systems, in: Proc. IEEE FIT, 2014.
[46] I. Fijalkow, C.E. Manlove, R. Johnson Jr., Adaptive fractionally spaced blind CMA equalization: excess MSE, IEEE Trans. Signal Process. 46 (1) (1998) 227–231.
[47] J.J. Shynk, R.P. Gooch, G. Krishnamurthy, C.K. Chan, Comparative performance study of several blind equalization algorithms, Proc. SPIE Conf. Adv. Signal Process. 1565 (2) (1991) 102–117.
[48] J. Mai, A.H. Sayed, A feedback approach to the steady-state performance of fractionally spaced blind adaptive equalizers, IEEE Trans. Signal Process. 48 (1) (2000) 80–91.
[49] N.R. Yousef, A.H. Sayed, A unified approach to the steady-state and tracking analyses of adaptive filters, IEEE Trans. Signal Process. 49 (2) (2001) 314–324.
[50] S. Abrar, A. Ali, A. Zerguine, A.K. Nandi, Tracking performance of two constant modulus equalizers, IEEE Commun. Lett. 17 (5) (2013) 830–833.
[51] S. Abrar, A.K. Nandi, Adaptive minimum entropy equalization algorithm, IEEE Commun. Lett. 14 (10) (2010) 966–968.
[52] A.W. Azim, S. Abrar, A. Zerguine, A.K. Nandi, Steady-state performance of multimodulus blind equalizers, Signal Process. 108 (2015) 509–520.
[53] N. Xie, H. Hu, H. Wang, A new hybrid blind equalization algorithm with steady-state performance analysis, Digit. Signal Process. 22 (2) (2012) 233–237.
[54] T. Thaiupathump, L. He, S.A. Kassam, Square contour algorithm for blind equalization of QAM signals, Signal Process. 86 (11) (2006) 3357–3370.
[55] S.A. Sheikh, P. Fan, New blind equalization techniques based on improved square contour algorithm, Digit. Signal Process. 18 (5) (2008) 680–693.
[56] S.A. Sheikh, P. Fan, Two efficient adaptively varying modulus blind equalizers: AVMA and DM/AVMA, Digit. Signal Process. 16 (6) (2006) 832–845.
[57] M.G. Larimore, J.R. Treichler, Convergence behavior of the constant modulus algorithm, in: Proc. IEEE ICASSP, vol. 8, 1983, pp. 13–16.
[58] V. Weerackody, S.A. Kassam, K.R. Laker, Sign algorithms for blind equalization and their convergence analysis, Circuits Syst. Signal Process. 10 (4) (1991) 393–431.
[59] T.Y. Al-Naffouri, A.H. Sayed, Adaptive filters with error nonlinearities: mean-square analysis and optimum design, EURASIP J. Appl. Signal Process. 1 (2001) 192–205.
[60] D. Dohono, On minimum entropy deconvolution, in: Proc. 2nd Applied Time Series Symp., 1980, pp. 565–608.
[61] M.T.M. Silva, M.D. Miranda, Tracking issues of some blind equalization algorithms, IEEE Signal Process. Lett. 11 (9) (2004) 760–763.
[62] N. Xie, H. Hu, H. Wang, A new hybrid blind equalization algorithm with steady-state performance analysis, Digit. Signal Process. 22 (2) (2012) 233–237.
[63] J. Mendes Filho, M.D. Miranda, M. Silva, A regional multimodulus algorithm for blind equalization of QAM signals: introduction and steady-state analysis, Signal Process. 92 (11) (2012) 2643–2656.
[64] M. Niroomand, M. Derakhtian, M.A. Masnadi-Shirazi, Steady-state performance analysis of a generalised multimodulus adaptive blind equalisation based on the pseudo Newton algorithm, IET Signal Process. 6 (1) (2012) 14–26.
[65] B. Lin, R. He, X. Wang, B. Wang, The excess mean-square error analyses for Bussgang algorithm, IEEE Signal Process. Lett. 15 (2008) 793–796.
[66] A. Goupil, J. Palicot, A geometrical derivation of the excess mean square error for Bussgang algorithms in a noiseless environment, Signal Process. 84 (2) (2004) 311–315.
[67] N. Gu, W. Yu, D. Creighton, S. Nahavandi, Selecting optimal norm and step size of generalised constant modulus algorithms under non-stationary environments, Electron. Lett. 46 (25) (2010) 1673–1674.
[68] S. Bellini, Bussgang techniques for blind deconvolution and equalization, in: Blind Deconvolution, Prentice Hall, Upper Saddle River, N.J., 1994.
[69] T.Y. Al-Naffouri, A.H. Sayed, Transient analysis of adaptive filters with error nonlinearities, IEEE Trans. Signal Process. 51 (3) (2003) 653–663.
[70] O. Dabeer, E. Masry, Convergence analysis of the constant modulus algorithm, IEEE Trans. Inf. Theory 49 (6) (2003) 1447–1464.
[71] P. Bello, Characterization of randomly time-variant linear channels, IEEE Trans. Commun. Syst. 11 (4) (1963) 360–393.
[72] C. Komninakis, C. Fragouli, A.H. Sayed, R.D. Wesel, Multi-input multi-output fading channel tracking and equalization using Kalman estimation, IEEE Trans. Signal Process. 50 (5) (2002) 1065–1076.
[73] G. Picchi, G. Prati, Blind equalization and carrier recovery using a "stop-and-go" decision-directed algorithm, IEEE Trans. Commun. 35 (9) (1987) 877–887.
[74] R. Raheli, G. Picchi, Synchronous and fractionally-spaced blind equalization in dually-polarized digital radio links, in: IEEE ICC, 1991, pp. 156–161.

Ali Waqar Azim received his Bachelor of Science in Electrical (Telecommunication) Engineering with distinction from COMSATS Institute of Information Technology, Islamabad, Pakistan. He obtained Diplôme d'ingénieur (Engineering Diploma) in Telecommunication Engineering and Laurea Magistrale in Ingegneria Elettronica (Masters in Electronic Engineering) from ENSIMAG, Institut Polytechnique de Grenoble, France, and Politechnico di Torino, Italy, respectively. Presently, he is working as a Lecturer at COMSATS Institute of Information Technology, Wah, Pakistan. His research interest is in Signal Processing and Digital Communications.

Shafayat Abrar was born in Karachi, Pakistan, in 1972. He holds a B.E. degree in electrical engineering from NED University of Engineering and Technology, Karachi, Pakistan (I996) and an M.S. degree in electrical engineering from King Fahd University of Petroleum and Minerals (KFUPM), Dhahran, Saudi Arabia (2000). He earned his Ph.D. degree in electrical engineering from The University of Liverpool, Liverpool, UK (2010). He has been co-recipient of *Best Paper Award of IEEE-INCC'04* at Lahore University of Management Sciences, Lahore, Pakistan. He has been co-recipient of *IEEE Communications Society Heinrich Hertz Award for Best Communications Letters* at IEEE GLOBECOM 2012 event in Anaheim, CA, USA.

Professor Azzedine Zerguine received the B.Sc. degree from Case Western Reserve University, Cleveland, OH, USA, in 1981, the M.Sc. degree from King Fahd University of Petroleum and Minerals (KFUPM), Dhahran, Saudi Arabia, in 1990, and the Ph.D. degree from Loughborough University, Loughborough, UK, in 1996, all in electrical engineering. He is currently a Professor in the Electrical Engineering Department, KFUPM, working in the areas of signal processing and communications. Dr. Zerguine was the recipient of three Best Teaching Awards, in 2000, 2005, and 2011 at KFUPM. He is presently serving as an Associate Editor of the EURASIP Journal on Advances in Signal Processing.

Professor Asoke K. Nandi received the degree of Ph.D. from the University of Cambridge (Trinity College), Cambridge (UK). He held academic positions in several universities, including Oxford (UK), Imperial College London (UK), Strathclyde (UK), and Liverpool (UK). In 2013 he moved to Brunel University (UK), to become the Chair and Head of Electronic and Computer Engineering. Professor Nandi is a Distinguished Visiting Professor at Tongji University (China), and an Adjunct Professor at University of Calgary (Canada).

His current research interests lie in the areas of signal processing and machine learning, with applications to communications, gene expression data, functional magnetic resonance data, and biomedical data. He has made many fundamental theoretical and algorithmic contributions to many aspects of signal processing and machine learning. He has much expertise in "Big Data", dealing with heterogeneous data, and extracting information from multiple datasets obtained in different laboratories and different times. He has authored over 500 technical publications, including 200 journal papers as well as four books.

Professor Nandi is a Fellow of the Royal Academy of Engineering and also a Fellow of seven other institutions including the IEEE and the IET. Among the many awards he received are the Institute of Electrical and Electronics Engineers (USA) Heinrich Hertz Award in 2012, the Glory of Bengal Award for his outstanding achievements in scientific research in 2010, the Water Arbitration Prize of the Institution of Mechanical Engineers (UK) in 1999, and the Mountbatten Premium, Division Award of the Electronics and Communications Division, of the Institution of Electrical Engineers (UK) in 1998.